and 24 hours later, 30 μl of cell suspensions containing 3×10^4 myoblasts, 3×10^4 CD31(−) CD45(−) SP cells, or 3×10^4 GFP(+) myoblasts plus 2×10^4 CD31(−) CD45(−) SP cells were directly injected into the TA muscles of 8-week-old *NOD/scid* or *mdx* mice. At several time points after transplantation, the muscles were dissected, fixed in 4% paraformaldehyde for 30 minutes, immersed in 10% sucrose/phosphate-buffered saline (PBS) and then in 20% sucrose/PBS, and frozen in isopentane cooled with liquid nitrogen.

Retrovirus Transduction in Vitro

Red fluorescent protein (DsRed) cDNA (BD Biosciences, San Diego, CA) was cloned into a retrovirus plasmid, pMXs, kindly provided by Dr. T. Kitamura of the University of Tokyo, Tokyo, Japan.[24] Viral particles were prepared by introducing the resultant pMXs-DsRed into PLAT-E retrovirus packaging cells,[25] and the filtered supernatant was added to the myoblast culture. The next day, DsRed(+) myoblasts were collected by flow cytometry.

Immunohistochemistry

We cut the entire TA muscle tissues on a cryostat into 6-μm cross sections, and observed all serial sections under fluorescence microscopy. We then selected two or three sections in which GFP(+) cells were found most frequently. The sections were then blocked with 5% goat serum (Cedarlane, Hornby, Canada) in PBS for 15 minutes, and then reacted with anti-GFP antibody (Chemicon International, Temecula, CA), anti-laminin α2 antibody (4H8-2; Alexis, San Diego, CA), anti-phospho-histone H3 antibody (Upstate Biotechnology, Lake Placid, NY), or anti-DsRed antibody (Clontech, Palo Alto, CA) at 4°C overnight. Dystrophin was detected using a monoclonal antibody, Dys-2 (Novocastra, Newcastle on Tyne, UK), and a M.O.M. Kit (Vector Laboratories, Burlingame, CA). The sections were then incubated with appropriate combinations of Alexa 488-, 568-, or 594-labeled secondary antibodies (Molecular Probes, Eugene, OR) and TOTO-3 (Molecular Probes), and photographed using a confocal laser-scanning microscope system TCSSP (Leica, Heidelberg, Germany). The area occupied by GFP(+) cells or myofibers was measured by using Image J software (National Institutes of Health, Bethesda, MD) on cross sections from three independent experiments, and defined as the distribution area.

RNA Isolation and Real-Time Polymerase Chain Reaction (PCR)

Total RNA was isolated from muscles using TRIzol (Invitrogen). First strand cDNA was synthesized using a QuantiTect reverse transcription kit (Qiagen, Hilden, Germany). The levels of GFP mRNA and 18S rRNA were quantified using SYBR Premix Ex Taq (Takara, Otsu, Shiga, Japan) on a MyiQ single-color system (Bio-Rad Laboratories, Richmond, CA) following the manufacturer's instructions. Primer sequences for real-time PCR were: 18s rRNA, forward: 5′-TACCCTGGCGGTGGGATTAAC-3′, reverse: 5′-CGAGAGAAGACCACGCCAAC-3′ and EGFP, forward: 5′-GACGTAAACGGCCACAAGTT-3′, reverse: 5′-AAGTCGTGCTGCTTCATGTG-3′. The expression levels of *MMP-2* and *MMP-9* were evaluated by conventional reverse transcriptase (RT)-PCR using the following primers: MMP-2, forward: 5′-TGCAAGGCAGTGGTCATAGCT-3′, reverse: 5′-AGCCAGTCGGATTTGATGCT-3′.

Cell Proliferation Assay

CD31(−) CD45(−) SP cells or 10T1/2 cells were cultured in Dulbecco's modified Eagle's medium containing 20% fetal bovine serum for 5 days, and the supernatants were collected as conditioned medium. Myoblasts were plated on 96-well culture plates at a density of 5000 cells/well and cultured in conditioned medium for 3 days. BrdU was then added to the culture medium (final concentration, 10 μmol/L). Twenty-four hours later, BrdU uptake was quantified by a cell proliferation enzyme-linked immunosorbent assay, a BrdU kit (Roche Diagnostics, Meylan, France), and Lumi-Image F1 (Roche).

Gene Expression Profiling

Total RNAs were extracted from CD31(−) CD45(−) SP cells, macrophages, or myoblasts using an RNeasy RNA isolation kit (Qiagen). cDNA synthesis, biotin-labeled target synthesis, MOE430A GeneChip (Affymetrix, Santa Clara, CA) array hybridization, staining, and scanning were performed according to standard protocols supplied by Affymetrix. The quality of the data presented in this study was controlled by using the Microarray Suite MAS 5.0 (Affymetrix). The MAS-generated raw data were uploaded to GeneSpring software version 7.0 (Silicon Genetics, Redwood City, CA). The software calculates signal intensities, and each signal was normalized to a median of its values in all samples or the 50th percentile of all signals in a specific hybridization experiment. Fold ratios were obtained by comparing normalized data of CD31(−) CD45(−) SP cells and macrophages or myoblasts.

In Situ *Zymography*

CD31(−) CD45(−) SP cells, myoblasts, and macrophages were isolated from regenerating muscles 3 days after CTX injection by cell sorting and collected by a Cytospin3 centrifuge (ThermoShandon, Cheshire, UK) on DQ-gelatin-coated slides (Molecular Probes). The slides were then incubated for 24 hours at 37°C in the presence or absence of GM6001 (a broad-spectrum inhibitor of MMPs, 50 μmol/L; Calbiochem, San Diego, CA) or E-64 (a cysteine protease inhibitor, 50 mmol/L; Calbiochem). Fluorescence of fluorescein isothiocyanate was detected with excitation at 460 to 500 nm and emission at 512 to 542 nm.

Statistics

Statistical differences were determined by Student's unpaired *t*-test. For comparison of more than two groups,

one-way analysis of variance was used. All values are expressed as means ± SE. A probability of less than 5% ($P < 0.05$) or 1% ($P < 0.01$) was considered statistically significant.

Results

Marker Expression on Muscle-Derived CD31(−) CD45(−) SP Cells

When incubated with 5 μg/ml of Hoechst 33342 dye at 37°C for 90 minutes, 1 to 3% of muscle mononuclear cells show the SP phenotype (Figure 1A). Previously, we reported that muscle SP cells can be further divided into three subpopulation, CD31(−) CD45(−) cells, CD31(−) CD45(+) cells, and CD31(+) CD45(−) SP cells (Figure 1B).[20] The CD31(−) CD45(−) SP cells did not express Pax3, Pax7, or Myf5, indicating that they are not yet committed to the muscle lineage.[20] RT-PCR suggested that CD31(−) CD45(−) SP cells have mesenchymal cell characteristics.[20] To further clarify the properties of CD31(−) CD45(−) SP cells, we analyzed their cell surface markers. CD31(−) CD45(−) SP cells were negative for CD124, CD133, CD14, c-kit (Figure 1B), and CD184 (data not shown), weakly positive for CD34 and CD49b, and strongly positive for Sca-1, CD44, and CD90 (Figure 1). The FACS patterns shown in Figure 1B suggested that CD31(−) CD45(−) SP cells are a homogeneous cell population. CD14 is an exception. A small fraction of CD31(−) CD45(−) SP cells were strongly positive for CD14, but the majority weakly expressed this marker. The function of CD14^{high} CD31(−) CD45(−) SP cells remains to be determined.

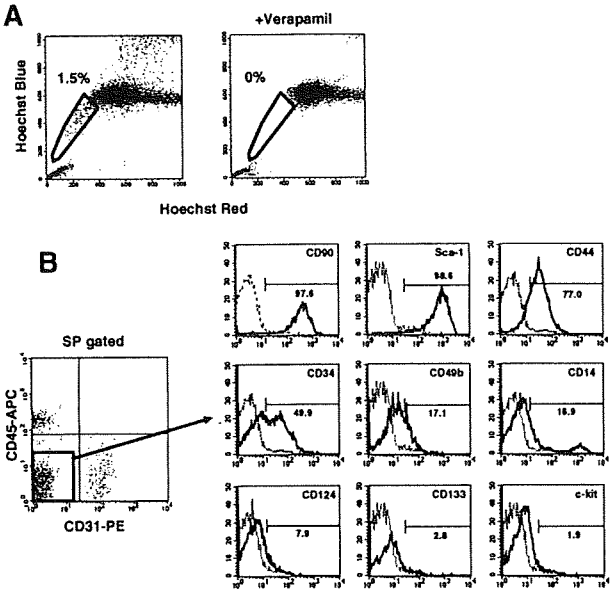

Figure 1. Cell surface markers on CD31(−) CD45(−) SP cells from regenerating muscle. **A:** Mononuclear cells were prepared from limb muscles of C57BL/6 mice at 3 days after CTX injection, incubated with 5 μmol/L Hoechst 33342 with (**right**) or without (**left**) Verapamil, and analyzed by a cell sorter. SP cells are shown by polygons. The numbers indicate the percentage of SP cells in all mononuclear cells. **B: Left:** Expression of CD45 and CD31 on muscle SP cells. **Right:** The expression of surface markers (CD90, Sca-1, CD44, CD34, CD49b, CD14, CD124, CD133, and c-kit) on CD31(−) CD45(−) SP cells was further analyzed by FACS. The *x* axis shows the fluorescence intensity, and the *y* axis indicates cell numbers. Solid lines are with antibodies; dotted lines are negative controls.

Efficiency of Myoblast Transplantation Is Increased by Co-Transplantation of Muscle CD31(−) CD45(−) SP Cells in NOD/scid Mice

To clarify the functions of CD31(−) CD45(−) SP cells during muscle regeneration, we isolated myoblasts from GFP-transgenic mice (GFP-Tg) and injected them (3×10^4 cells/muscle) with or without CD31(−) CD45(−) SP cells (2×10^4 cells/muscle) into TA muscles of immunodeficient *NOD/scid* mice (Figure 2A). CTX was injected into recipient muscles 24 hours before cell transplantation to induce muscle regeneration. Two weeks after transplantation, the contribution of grafted myoblasts to muscle regeneration was investigated by immunodetection of GFP(+) myofibers. Co-transplantation of GFP(+) myoblasts with nonlabeled CD31(−) CD45(−) SP cells produced a higher number of GFP(+) myofibers than transplantation of GFP(+) myoblasts alone (Figure 2, B and C). Furthermore, the average diameter of GFP(+) myofibers was significantly larger in co-transplanted muscles than in muscles transplanted with myoblasts alone (Figure 2D). These results suggest that more myoblasts participated in myofiber formation after co-transplantation than after single transplantation, injected SP cells promoted growth of regenerating myofibers, or both.

Co-transplantation of Myoblasts with Muscle CD31(−) CD45(−) SP Cells Significantly Increased Efficiency of Myoblast Transplantation in mdx Mice

Next, co-transplantation experiments were performed using 8-week-old dystrophin-deficient *mdx* mice as a host. Three kinds of transplantations were performed: 3×10^4 myoblasts derived from GFP-Tg mice, 3×10^4 CD31(−) CD45(−) SP cells derived from GFP-Tg mice, or a mixture of GFP(+) 3×10^4 myoblasts and 2×10^4 CD31(−) CD45(−) SP cells derived from C57BL/6 mice (Figure 3A).

When analyzed at 2 weeks after transplantation, a much higher number of GFP(+) myofibers were detected on cross-sections after co-transplantation of myoblasts and CD31(−) CD45(−) SP cells than after transplantation of GFP(+) myoblasts alone (Figure 3, B and C). On the other hand, transplantation of GFP(+) SP cells alone resulted in formation of few GFP(+) myofibers. This observation is consistent with our previous report.[20] Co-transplantation of myoblasts and CD31(−) CD45(−) SP cells also gave rise to more myofibers expressing dystrophin at the sarcolemma in dystrophin-deficient *mdx* muscles than transplantation of myoblasts alone (data not shown). Again, the diameter of GFP(+) myofibers was significantly larger in co-transplanted muscles than in muscles transplanted with myoblasts or CD31(−) CD45(−) SP cells alone (Figure 3D).

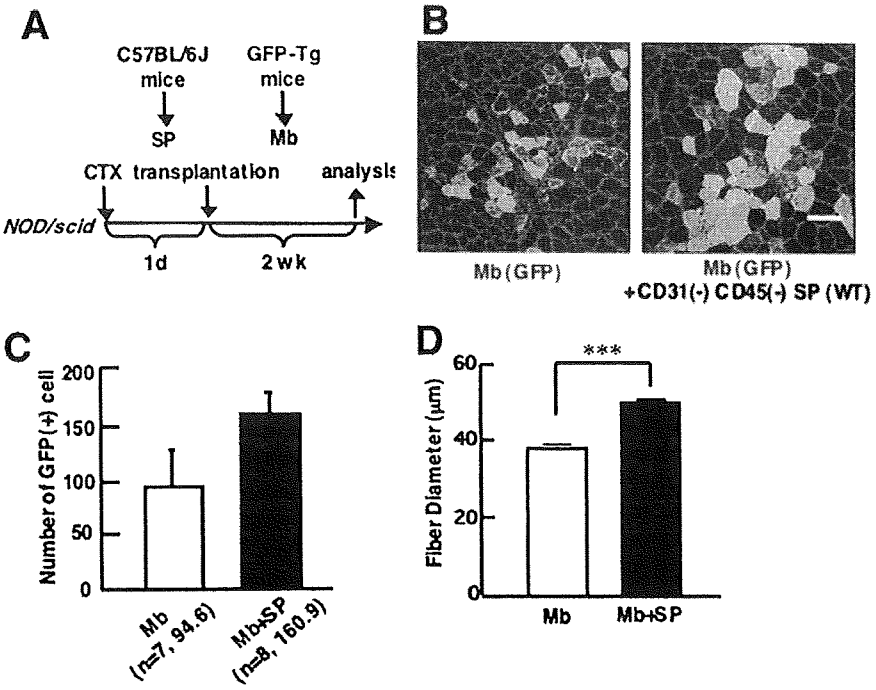

Figure 2. Co-transplantation of myoblasts and CD31(−) CD45(−) SP cells into skeletal muscle of immunodeficient *NOD/scid* mice promotes myofiber formation by transplanted myoblasts. **A:** Schematic protocol of co-transplantation experiments. CTX was injected into TA muscle 1 day before transplantation. Then, GFP(+) myoblasts (Mb) alone or with a mixture of GFP(+) myoblasts and CD31(−) CD45(−) SP cells derived from wild-type (WT) mice were transplanted to CTX-injected TA muscles of 8- to 12-week-old *NOD/scid* mice, and sampled 2 weeks after transplantation. **B:** Cross-sections of transplanted TA muscles stained with anti-GFP (green) and anti-laminin-α2 chain (red) antibodies. Nuclei were stained with TOTO3 (blue). **C:** The number of GFP(+) fibers per cross section of transplanted TA muscle. Values are means with SE (seven to eight mice in each group). $^{**}P < 0.01$. **D:** Average diameters of GFP(+) fibers in the TA muscles transplanted with myoblasts (Mb) or myoblasts plus CD31(−) CD45(−) SP cells (Mb + SP). Values are means with SE. $^{***}P < 0.001$. Scale bar = 80 μm.

The transplantation efficiency of myoblasts in *mdx* mice was 40 to 60% lower than that in *NOD/scid* mice. In the present study, *mdx* mice were not treated with any immunosuppressant. Although cellular infiltration was not evident when examined 2 weeks after transplantation (data not shown), some immune reaction might be evoked and eliminate myoblasts transplanted into *mdx* muscle.

Localization of Transplanted Myoblasts and CD31(−) CD45(−) SP Cells after Intramuscular Injection

To examine the interaction between grafted myoblasts and CD31(−) CD45(−) SP cells during muscle regeneration, we labeled C57BL/6 myoblasts with a retrovirus vector expressing a red fluorescent protein, DsRed. CD31(−) CD45(−) SP cells were isolated from GFP-Tg mice. We then injected a mixture of DsRed(+) myoblasts and GFP(+) CD31(−) CD45(−) SP cells into CTX-injected *NOD/scid* TA muscles. At 24 hours after transplantation, DsRed(+) myoblasts and GFP(+) CD31(−) CD45(−) SP cells were observed clearly (Figure 4A). At 48 hours after transplantation, immunohistochemistry revealed that grafted CD31(−) CD45(−) SP cells expanded, and surrounded both grafted myoblasts and damaged myofibers, but rarely fused with myoblasts (Figure 4B).

CD31(−) CD45(−) SP Cells Promote Proliferation of Myoblasts in Vivo *and* in Vitro

Next, to clarify the mechanism by which co-transplanted CD31(−) CD45(−) SP cells increased the contribution of grafted myoblasts to myofiber regeneration, we investigated the survival of grafted myoblasts after transplantation (Figure 5). GFP(+) myoblasts were injected into TA muscles of *NOD/scid* mice with or without unlabeled CD31(−) CD45(−) SP cells. At 24, 48, and 72 hours after transplantation, injected TA muscles were dissected, and the GFP mRNA level in injected muscles was evaluated by using real-time PCR (Figure 5A). There was a decline of the GFP mRNA level of injected muscles from 24 to 72 hours after injection (Figure 5B) with no differences in survival rates between single transplantation and co-transplantation.

At 48 and 72 hours after transplantation, however, GFP mRNA levels were slightly higher in co-injected muscle than in muscle injected with myoblasts alone (Figure 5B). Therefore, we directly counted the number of GFP(+) myoblasts at 72 hours after transplantation. As shown in Figure 6, A and B, many more GFP(+) myoblasts were detected in co-transplanted muscles than in myoblast-transplanted muscles (Figure 6, A and B). In addition, GFP(+) cells were more widely spread in the co-injected muscles than in muscles transplanted with myoblasts alone (Figure 6C).

To determine whether CD31(−) CD45(−) SP cells promote proliferation of implanted myoblasts, we dissected the muscles at 48 hours after transplantation, and stained the cross-sections with anti-phosphorylated histone H3 antibody, a marker of the mitotic phase of the cell cycle. Co-transplantation of myoblasts with CD31(−) CD45(−) SP cells significantly increased the percentage of mitotic GFP(+) cells compared with transplantation of myoblasts alone (Figure 6D). These observations suggest that co-injection of CD31(−) CD45(−) SP cells promoted proliferation of grafted myoblasts.

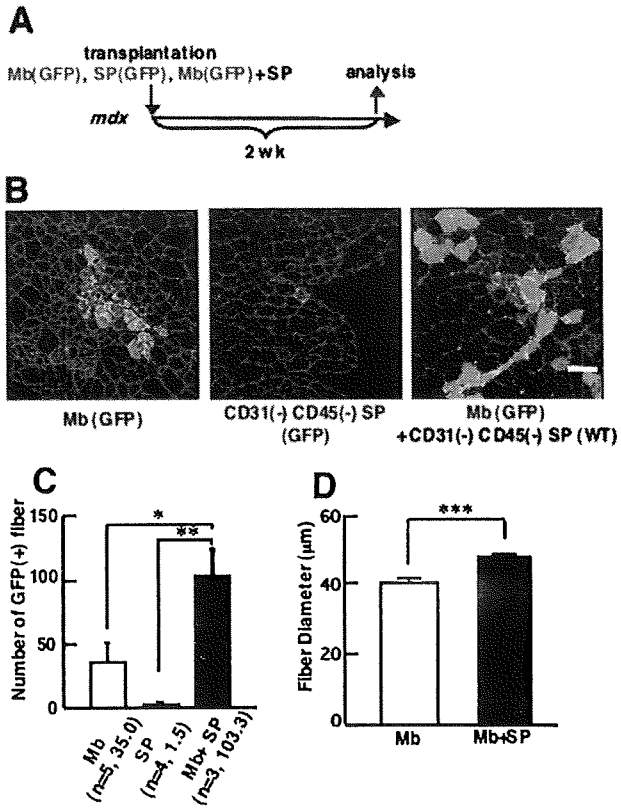

Figure 3. Co-transplantation of CD31(−) CD45(−) SP cells and myoblasts improves efficiency of myoblast transfer in dystrophin-deficient *mdx* mice. **A:** Schematic protocol of experiments. GFP(+) myoblasts alone (3×10^4), GFP(+) CD31(−) CD45(−) SP cells alone (3×10^4 cells), or a mixture of GFP(+) myoblasts (3×10^4) and CD31(−) CD45(−) SP cells (2×10^4) were directly injected into TA muscles of 8-week-old *mdx* mice, and the muscles were sampled 2 weeks after transplantation. **B:** Cross-sections of transplanted TA muscles stained with anti-GFP (green) and anti-laminin-α2 chain (red) antibodies. Nuclei were stained with TOTO3 (blue). **C:** The number of GFP(+) fibers per cross section. Myoblasts gave rise to more myofibers when co-transplanted with CD31(−) CD45(−) SP cells (Mb + SP) than when transplanted alone (Mb). Transplantation of only GFP(+) SP cells resulted in formation of few myofibers (SP). Values are means with SE (n = 3 to 5 mice). $^*P < 0.05$, $^{**}P < 0.01$. **D:** Average diameters of GFP(+) fibers in the TA muscles transplanted with myoblasts (Mb) or with myoblasts plus CD31(−) CD45(−) SP cells (Mb + SP). Values are means with SE. $^{***}P < 0.001$. Scale bar = 80 μm.

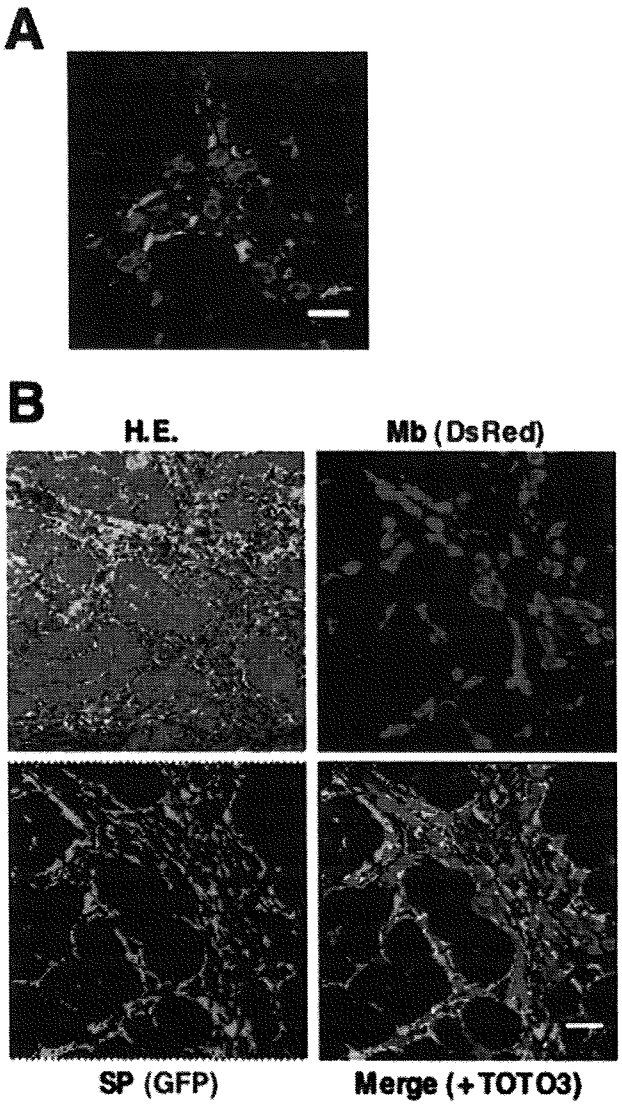

Figure 4. Behavior of GFP$^+$ CD31(−) CD45(−) SP cells and DsRed-labeled myoblasts after transplantation. **A:** *NOD/scid* TA muscles were injected with CTX 24 hours before transplantation. Then, myoblasts transduced with a retrovirus vector expressing DsRed were injected together with GFP(+) CD31(−) CD45(−) SP cells into the muscles. The muscles were dissected 24 hours after the transplantation, sectioned, and stained with anti-DsRed (red) and anti-GFP antibodies (green). Nuclei were stained with TOTO3 (blue). **B:** Representative image of DsRed(+) myoblasts and GFP(+) SP cells 48 hours after co-transplantation. One serial section was stained with H&E. Scale bars = 40 μm.

Next, to examine whether CD31(−) CD45(−) SP cells directly promote proliferation of myoblasts or not, we performed an *in vitro* proliferation assay using primary myoblasts and conditioned medium (CM) of CD31(−) CD45(−) SP cells and CM of 10T1/2 cells. BrdU uptake analysis showed that SP-CM more strongly stimulated the proliferation of myoblasts than 10T1/2-CM did (Figure 6E). The results suggest that CD31(−) CD45(−) SP cells promote proliferation of injected myoblasts at least in part by producing soluble factors.

Gene Expression Profiling of CD31(−) CD45(−) SP Cells

To identify the growth factor produced by CD31(−) CD45(−) SP cells that promotes proliferation of myoblasts, we extracted total RNAs from CD31(−) CD45(−) SP cells, myoblasts, and macrophages isolated from regenerating muscles 3 days after CTX injection, and examined the gene expression in these three cell populations by microarray. Eventually, we identified 192 genes that were expressed at more than 10-fold higher levels in CD31(−) CD45(−) SP cells than in either macrophages or myoblasts. We categorized the 192 genes based on gene ontology, and found that CD31(−) CD45(−) SP cells preferentially express extracellular matrix proteins and cytokines and their receptors (see Supplementary Table S1 at *http://ajp.amjpathol.org*). We found numerous genes involved in wound healing and tissue repair on the gene list, suggesting that CD31(−) CD45(−) SP cells play a regulatory role in the muscle regeneration process. Interestingly, the gene list contained both muscle prolif-

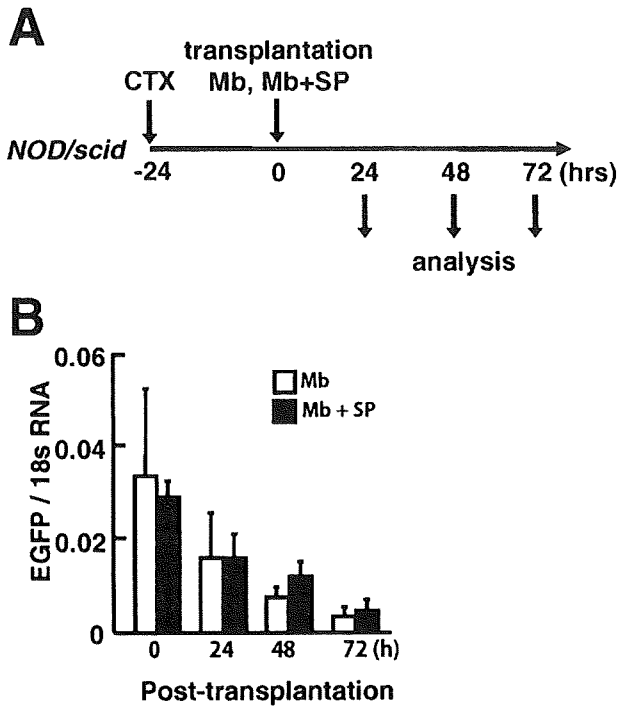

Figure 5. Survival of injected myoblasts in *NOD/scid* mice. **A:** Experimental design. GFP(+) myoblasts alone (3×10^4 cells) or a mixture of GFP(+) myoblasts (3×10^4 cells) and nonlabeled CD31(−) CD45(−) SP cells (2×10^4 cells) were injected into previously CTX-injected TA muscles of *NOD/scid* mice. The muscles were then sampled at 0, 24, 48, and 72 hours after transplantation. **B:** The mRNA level of GFP at each time point was quantified by real-time PCR. The *y* axis shows GFP mRNA levels normalized to 18s RNA with SE ($n = 4$ to 5).

eration or differentiation-promoting (follistatin),[26] and inhibitory factors (eg, insulin-like growth factor binding proteins,[27] Nov[28]). The list also contains regulators of TGF-β (eg, thrombospondins,[29] Prss11,[30] Ltbp3[31]), which would consequently attenuate or stimulate proliferation and differentiation of myoblasts.

CD31(−) CD45(−) SP Cell-Derived MMP-2 Promotes the Migration of Myoblasts

Genome-wide gene expression analysis revealed that CD31(−) CD45(−) SP cells highly express matrix metalloproteinases (see Supplementary Table S1 and Supplementary Figure S1 at *http://ajp.amjpathol.org*). MMPs are a group of zinc-dependent endopeptidases that degrade extracellular matrix components, thereby facilitating cell migration and tissue remodeling.[32,33] Furthermore, MMPs are known to release growth factors stored within the extracellular matrix and process growth factor receptors, resulting in stimulation of cell proliferation.[34–36] Among the MMPs up-regulated in CD31(−) CD45(−) SP cells, we paid special attention to MMP-2 (also called gelatinase A or 72-kDa type IV collagenase). In CTX-injected muscle, MMP-2 activity was shown to be increased concomitantly with the transition from the regeneration phases characterized by the appearance of young myotubes to maturation of the myotubes into multinucleated myofibers[37,38] MMP-2 was also activated in the endomysium of regenerating fibers in dystrophin-deficient muscular dystrophy dogs.[39] Furthermore, MMP-2 transcripts were found in the areas of fiber regeneration, and were localized to mesenchymal fibroblasts in DMD skeletal muscle.[40]

We confirmed that the mRNA level of MMP-2 was much higher in CD31(−) CD45(−) SP cells than in macrophages or myoblasts (Figure 7A). Next, we examined the gelatinolytic activity in CD31(−) CD45(−) SP cells, macrophages, and myoblasts by DQ-gelatin zymography. The cells were directly isolated from regenerating muscle. High gelatinolytic activity was detected in CD31(−) CD45(−) SP cells, compared to myoblasts or macrophages (Figure 7B). Importantly, the signal in MMP-2-null SP cells was considerably weak, compared with wild-type SP cells. The results indicate that DQ-gelatin was degraded mainly (but not exclusively) by MMP-2 in the assay. We hardly detected the green fluorescence in wild-type SP cells in the presence of a broad-spectrum inhibitor of MMPs, GM6001, but not a potent inhibitor of cysteine proteases, E-64, suggesting that other MMPs contribute to gelatin degradation to some extent in the assay. Collectively, these results indicate that CD31(−) CD45(−) SP cells have high MMP-2 activity.

MMP-2 is reported to mediate cell migration and tissue remodeling.[32,33] To directly investigate the effects of MMP-2 on the migration and proliferation of transplanted myoblasts, we injected GFP(+) myoblasts with CD31(−) CD45(−) SP cells prepared from wild-type mice or from MMP-2-null mice into CTX-injected TA muscles of *NOD/scid* mice. There was no difference in the yield of CD31(−) CD45(−) SP cells from regenerating muscle between wild-type and MMP-2-null mice (data not shown). Consistent with this observation, MMP-2-null CD31(−) CD45(−) SP cells proliferated as vigorously as wild-type *in vitro* (data not shown). At 72 hours after transplantation, GFP(+) myoblasts were more widely spread in the muscle co-injected with wild-type CD31(−) CD45(−) SP cells than in the muscles co-injected with MMP-2-deficient CD31(−) CD45(−) SP cells (Figure 7C). In contrast, there was no difference in the number of GFP(+) myoblasts between two groups (Figure 7D). These results strongly suggest that MMP-2 derived from CD31(−) CD45(−) SP cells significantly promotes migration of myoblasts, but does not influence the proliferation of myoblasts.

Discussion

We previously reported a novel SP subset: CD31(−) CD45(−) SP cells.[20] They are resident in skeletal muscle and are activated and vigorously proliferate during muscle regeneration. RT-PCR analysis suggested that CD31(−) CD45(−) SP cells are of mesenchymal lineage, and indeed they differentiated into adipocytes, osteogenic cells, and muscle cells after specific induction *in vitro*.[20] In the present study, we further characterized CD31(−) CD45(−) SP cells and found that co-transplantation of CD31(−) CD45(−) SP cells markedly improves the efficacy of myoblast transfer to dystrophic *mdx* mice. Our

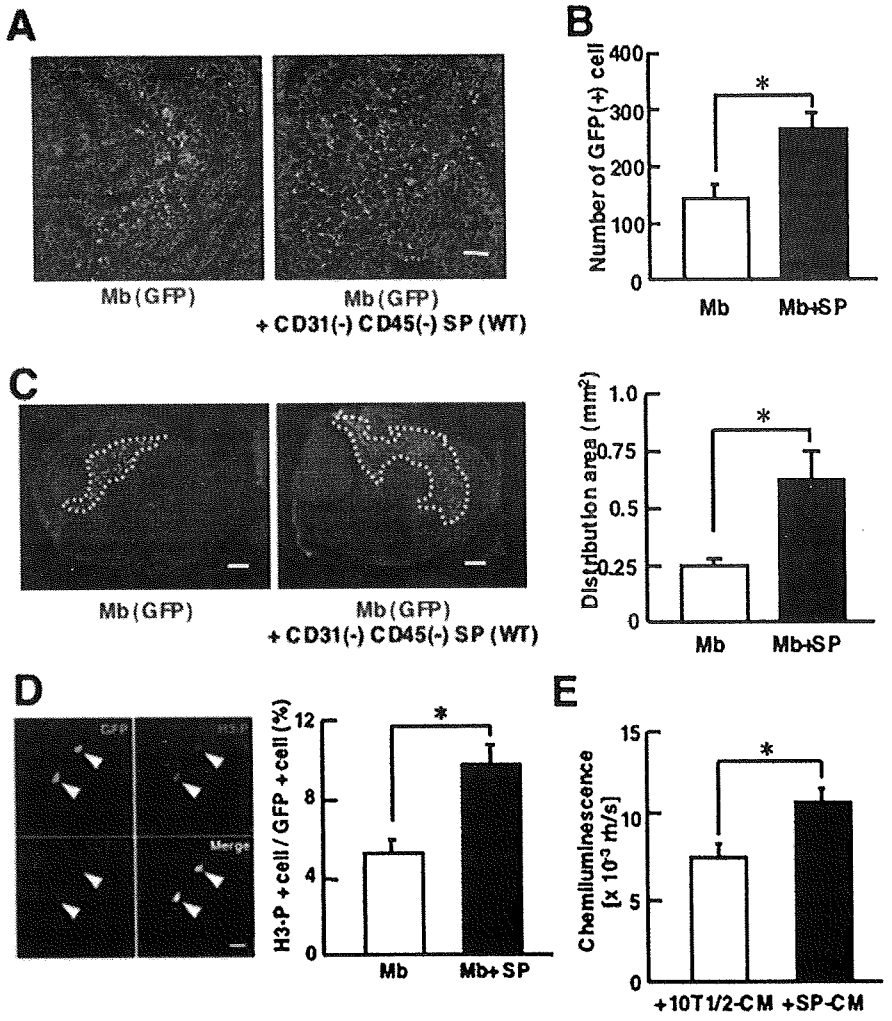

Figure 6. CD31(−) CD45(−) SP cells promote proliferation of myoblasts *in vitro* and *in vivo*. **A:** Representative images of cross sections of 72-hour samples stained with anti-GFP (green) and anti-laminin-α2 chain (red) antibodies. GFP(+) myoblasts are more widely scattered in injected muscle when co-transplanted with CD31(−) CD45(−) SP cells, compared with single transplantation. **B:** The number of GFP(+) cells per cross section of TA muscles injected with myoblasts or myoblasts and CD31(−) CD45(−) SP cells. Values were means with SE (n = 4 to 5). $^*P < 0.05$. **C: Left:** Representative distributions of GFP(+) myoblasts/myotubes 72 hours after transplantation. **Right:** Distribution area (marked by white dotted lines in **left** panels) was measured by Image J software. Values were means with SE (n = 4 to 5). $^*P < 0.05$. **D:** GFP(+) myoblasts were transplanted into CTX-injected TA muscles of *NOD/scid* mice with (Mb + SP) or without CD31(−) CD45(−) SP cells (Mb). Forty-eight hours after transplantation, the muscles were dissected, sectioned, and stained with anti-phosphorylated histone-H3 (H3-P) (red) and anti-GFP (green) antibodies. **Arrowheads** indicate H3-P(+) GFP(+) cells. The **right** graph shows the percentage of H3-P(+) cells in GFP(+) myoblasts in single-transplanted muscle (Mb) or in co-transplanted muscle (Mb + SP). The values are means with SE (n = 3). $^*P < 0.05$. **E:** Myoblasts were cultured for 3 days in conditioned medium of either CD31(−) CD45(−) SP cells (SP-CM) or 10T1/2 cells (10T1/2-CM) and then cultured for an additional 24 hours in the presence of BrdU. The vertical axis shows BrdU uptake by myoblasts. Values are means with SE (n = 6). $^*P < 0.05$. Scale bars: 100 μm (**A**); 200 μm (**C**); 80 μm (**D**).

findings suggest that endogenous CD31(−) CD45(−) SP cells support muscle regeneration by stimulating proliferation and migration of myoblasts.

Are CD31(−) CD45(−) SP Cells Mesenchymal Stem Cells?

Analysis of cell surface antigens on CD31(−) CD45(−) SP cells suggests that they are a homogeneous population. Several reports showed that mesenchymal stem cells (MSCs) express CD44, CD90, but not CD31, CD45, or CD14.[41,42] The expression patterns of these markers on CD31(−) CD45(−) SP cells and their differentiation potentials into osteogenic cells, adipocytes, and myogenic cells suggest that CD31(−) CD45(−) SP cells are closely related to MSCs.[20] On the other hand, the expression of PDGFRβ,[20] CD44, CD49b, CD90, and the lack of CD133 expression on CD31(−) CD45(−) SP cells are similar to those of human pericytes.[13] Unlike human pericytes, however, CD31(−) CD45(−) SP cells have limited myogenic potential *in vivo*.[13,20] The relationship between CD31(−) CD45(−) SP cells and MSCs or pericytes remains to be determined in a future study.

CD31(−) CD45(−) SP Cells Promote Proliferation of Myogenic Cells

In the present study, we demonstrated that the efficiency of myoblast transfer is greatly improved by co-transplantation of CD31(−) CD45(−) SP cells. Transplanted CD31(−) CD45(−) SP cells proliferated in the injection site and surrounded both engrafted myoblasts and damaged myofibers, but rarely fused with myoblasts (Figure 4). Transplantation of CD31(−) CD45(−) SP cells alone contributed little to myofiber formation. Therefore, the improvement in efficiency of myoblast transfer by co-transplantation is not attributable to differentiation of CD31(−) CD45(−) SP cells into muscle fibers.

Because the conditioned medium from CD31(−) CD45(−) SP cells modestly stimulated the proliferation of myoblasts *in vitro*, when compared with CM of 10T1/2 cells, it is possible that CD31(−) CD45(−) SP cells stimulated proliferation of myoblasts by secreting growth factors. CD31(−) CD45(−) SP cells are found in close vicinity to myoblasts 48 hours after transplantation. Therefore, even low levels of growth factors produced by CD31(−) CD45(−) SP cells may effectively stimulate the prolifera-

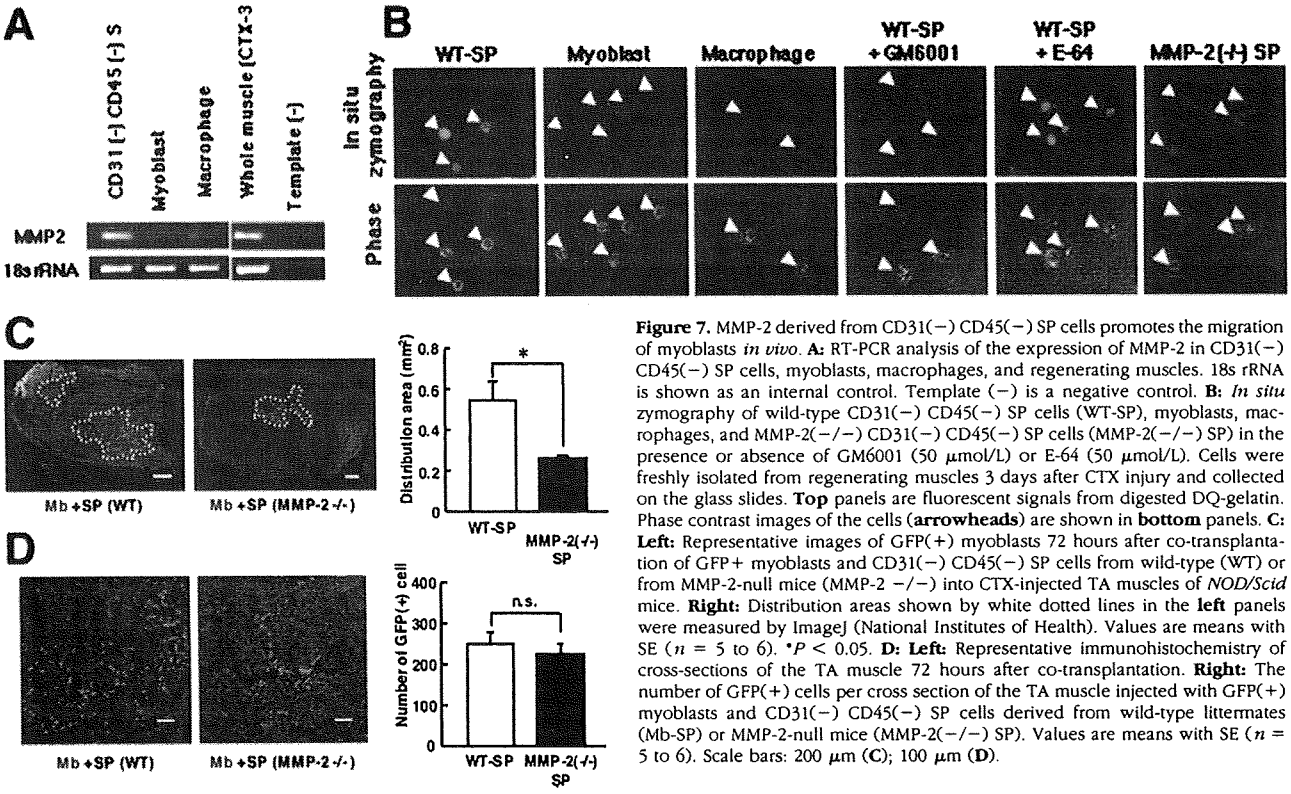

Figure 7. MMP-2 derived from CD31(−) CD45(−) SP cells promotes the migration of myoblasts *in vivo*. **A:** RT-PCR analysis of the expression of MMP-2 in CD31(−) CD45(−) SP cells, myoblasts, macrophages, and regenerating muscles. 18s rRNA is shown as an internal control. Template (−) is a negative control. **B:** *In situ* zymography of wild-type CD31(−) CD45(−) SP cells (WT-SP), myoblasts, macrophages, and MMP-2(−/−) CD31(−) CD45(−) SP cells (MMP-2(−/−) SP) in the presence or absence of GM6001 (50 μmol/L) or E-64 (50 μmol/L). Cells were freshly isolated from regenerating muscles 3 days after CTX injury and collected on the glass slides. **Top** panels are fluorescent signals from digested DQ-gelatin. Phase contrast images of the cells (**arrowheads**) are shown in **bottom** panels. **C: Left:** Representative images of GFP(+) myoblasts 72 hours after co-transplantation of GFP+ myoblasts and CD31(−) CD45(−) SP cells from wild-type (WT) or from MMP-2-null mice (MMP-2 −/−) into CTX-injected TA muscles of *NOD/Scid* mice. **Right:** Distribution areas shown by white dotted lines in the **left** panels were measured by ImageJ (National Institutes of Health). Values are means with SE (n = 5 to 6). $^*P < 0.05$. **D: Left:** Representative immunohistochemistry of cross-sections of the TA muscle 72 hours after co-transplantation. **Right:** The number of GFP(+) cells per cross section of the TA muscle injected with GFP(+) myoblasts and CD31(−) CD45(−) SP cells derived from wild-type littermates (Mb-SP) or MMP-2-null mice (MMP-2(−/−) SP). Values are means with SE (n = 5 to 6). Scale bars: 200 μm (**C**); 100 μm (**D**).

tion of myoblasts. Importantly, several reports showed that MSCs secrete a variety of cytokines and growth factors, which suppress the local immune system, inhibit fibrosis and apoptosis, enhance angiogenesis, and stimulate mitosis and differentiation of tissue-specific stem cells.[43] On the gene list, we found a variety of cytokines/chemokines and their regulators (see Supplementary Table S1 at *http://ajp.amjpathol.org*). These molecules may directly or indirectly stimulate proliferation of myoblasts.

MMP-2 Derived from CD31(−) CD45(−) SP Cells Promotes the Migration of Myoblasts

Transplanted GFP(+) myoblasts were more widely spread in injected muscle when co-injected with CD31(−) CD45(−) SP cells than when transplanted alone (Figure 6C). MMP-2 is a candidate molecule that promotes migration of myoblasts. MMP-2 plays a critical role in myogenesis[44] and is up-regulated in muscle regeneration (see Supplementary Figure S2 at *http://ajp.amjpathol.org*).[38] MMP-2 expression is also detected in regenerating areas of dystrophic muscles.[39,40] Importantly, El Fahime and colleagues[45] reported that forced expression of MMP-2 in normal myoblasts significantly increased migration of myoblasts *in vivo*. In the present study, we demonstrated that CD31(−) CD45(−) SP cells highly express MMP-2 (see Figure 7A and Supplementary Table S1 at *http://ajp.amjpathol.org*). Gelatin zymography confirmed that CD31(−) CD45(−) SP cells have high gelatinolytic activities (Figure 7B). Importantly, CD31(−) CD45(−) SP cells prepared from wild-type mice promoted the migration of transplanted myoblasts, but those from MMP-2-null mice did not (Figure 7C). Our results suggest that CD31(−) CD45(−) SP cells promote the migration of myoblasts via MMP-2 secretion. CD31(−) CD45(−) SP cells highly express MMP-2, 3, 9, 14, and 23 during regenerating muscle (see Supplementary Figures S1 and S2 and Supplementary Table S1 at *http://ajp.amjpathol.org*). Therefore, it remains to be determined whether MMPs other than MMP-2 also promote the migration of myoblasts. MMPs are reported to promote cell proliferation by releasing local growth factors stored within the extracellular matrix and process growth factor receptors.[34,35,46] In the present study, however, MMP-2 derived from CD31(−) CD45(−) SP cells did not stimulate the proliferation of myoblasts *in vivo* (Figure 7D). The factors that stimulate the proliferation of myoblasts remain to be determined in a future study. MMP-3, -9, -14, and -23 are candidates that play a role in stimulating the proliferation of myoblasts.

CD31(−) CD45(−) SP Cells Are the Third Cellular Component of Muscle Regeneration

Our results suggest that transplanted CD31(−) CD45(−) SP cells stimulate myogenesis of co-transplanted myoblasts by supporting their proliferation and migration. Our results also suggest that endogenous CD31(−) CD45(−) SP cells promote muscle regeneration by the same mechanisms. Muscle regeneration is a complex, highly coordinated process in which not only myogenic cells but also inflammatory cells such as macrophages play critical roles.[3] Based on our finding that CD31(−) CD45(−) SP cells regulate myoblast proliferation and migration, we

propose that CD31(−) CD45(−) SP cells are a third cellular component of muscle regeneration. In addition, gene expression analysis on CD31(−) CD45(−) SP cells revealed that CD31(−) CD45(−) SP cells express a wide range of regulatory molecules implicated in embryonic development, tissue growth and repair, angiogenesis, and tumor progression, suggesting that CD31(−) CD45(−) SP cells are a versatile player in regeneration of skeletal muscle. Future studies of ablation of endogenous CD31(−) CD45(−) SP cells in the mouse will likely further clarify the mechanisms by which CD31(−) CD45(−) SP cells promote muscle regeneration.

Acknowledgments

We thank Satoru Masuda and Chika Harano for technical support.

References

1. Chargé SB, Rudnicki MA: Cellular and molecular regulation of muscle regeneration. Physiol Rev 2004, 84:209–238
2. Orimo S, Hiyamuta E, Arahata K, Sugita H: Analysis of inflammatory cells and complement C3 in bupivacaine-induced myonecrosis. Muscle Nerve 1991, 14:515–520
3. Tidball JG: Inflammatory processes in muscle injury and repair. Am J Physiol 2005, 288:R345–R353
4. Mauro A: Satellite cell of skeletal muscle fibers. J Biophys Biochem Cytol 1961, 9:493–495
5. Collins CA, Olsen I, Zammit PS, Heslop L, Petrie A, Partridge TA, Morgan JE: Stem cell function, self-renewal, and behavioral heterogeneity of cells from the adult muscle satellite cell niche. Cell 2005, 122:289–301
6. Kuang S, Kuroda K, Le Grand F, Rudnicki MA: Asymmetric self-renewal and commitment of satellite stem cells in muscle. Cell 2007, 129:999–1010
7. Qu-Petersen Z, Deasy B, Jankowski, R, Ikezawa M, Cummins J, Pruchnic R, Mytinger J, Cao B, Gates C, Wernig A, Huard J: Identification of a novel population of muscle stem cells in mice: potential for muscle regeneration. J Cell Biol 2002, 157:851–864
8. Jiang Y, Vaessen B, Lenvik T, Blackstad M, Reyes M, Verfaillie CM: Multipotent progenitor cells can be isolated from postnatal murine bone marrow, muscle, and brain. Exp Hematol 2002, 30:896–904
9. Tamaki T, Akatsuka A, Ando K, Nakamura Y, Matsuzawa H, Hotta T, Roy RR, Edgerton VR: Identification of myogenic-endothelial progenitor cells in the interstitial spaces of skeletal muscle. J Cell Biol 2002, 157:571–577
10. Torrente Y, Tremblay JP, Pisati F, Belicchi M, Rossi B, Sironi M, Fortunato F, El Fahime M, D'Angelo MG, Caron NJ, Constantin G, Paulin D, Scarlato G, Bresolin N: Intraarterial injection of muscle-derived CD34(+)Sca-1(+) stem cells restores dystrophin in mdx mice. J Cell Biol 2001, 152:335–348
11. Polesskaya A, Seale P, Rudnicki MA: Wnt signaling induces the myogenic specification of resident CD45+ adult stem cells during muscle regeneration. Cell 2003, 113:841–852
12. Sampaolesi M, Blot S, D'Antona G, Granger N, Tonlorenzi R, Innocenzi A, Mognol P, Thibaud JL, Galvez BG, Barthelemy I, Perani L, Mantero S, Guttinger M, Pansarasa O, Rinaldi C, Cusella De Angelis MG, Torrente Y, Bordignon C, Bottinelli R, Cossu G: Mesoangioblast stem cells ameliorate muscle function in dystrophic dogs. Nature 2006, 444:574–579
13. Dellavalle A, Sampaolesi M, Tonlorenzi R, Tagliafico E, Sacchetti B, Perani L, Innocenzi A, Galvez BG, Messina G, Morosetti R, Li S, Belicchi M, Peretti G, Chamberlain JS, Wright WE, Torrente Y, Ferrari S, Bianco P, Cossu G: Pericytes of human skeletal muscle are myogenic precursors distinct from satellite cells. Nat Cell Biol 2007, 9:255–267
14. Goodell MA, Brose K, Paradis G, Conner AS, Mulligan RC: Isolation and functional properties of murine hematopoietic stem cells that are replicating in vivo. J Exp Med 1996, 183:1797–1806
15. Gussoni E, Soneoka Y, Strickland CD, Buzney EA, Khan MK, Flint AF, Kunkel LM, Mulligan RC: Dystrophin expression in the mdx mouse restored by stem cell transplantation. Nature 1999, 401:390–394
16. Jackson KA, Mi T, Goodell MA: Hematopoietic potential of stem cells isolated from murine skeletal muscle. Proc Natl Acad Sci USA 1999, 96:14482–14486
17. Asakura A, Seale P, Girgis-Gabardo A, Rudnicki MA: Myogenic specification of side population cells in skeletal muscle. J Cell Biol 2002, 159:123–134
18. Bachrach E, Perez AL, Choi YH, Illigens BM, Jun SJ, del Nido P, McGowan FX, Li S, Flint A, Chamberlain J: Muscle engraftment of myogenic progenitor cells following intraarterial transplantation. Muscle Nerve 2006, 34:44–52
19. Frank NY, Kho AT, Schatton T, Murphy GF, Molloy MJ, Zhan Q, Ramoni MF, Frank MH, Kohane IS, Gussoni E: Regulation of myogenic progenitor proliferation in human fetal skeletal muscle by BMP4 and its antagonist Gremlin. J Cell Biol 2006, 175:99–110
20. Uezumi A, Ojima K, Fukada S, Ikemoto M, Masuda S, Miyagoe-Suzuki Y, Takeda S: Functional heterogeneity of side population cells in skeletal muscle. Biochem Biophys Res Commun 2006, 341:864–873
21. Ojima K, Uezumi A, Miyoshi H, Masuda S, Morita Y, Fukase A, Hattori A, Nakauchi H, Miyagoe-Suzuki Y, Takeda S: Mac-1(low) early myeloid cells in the bone marrow-derived SP fraction migrate into injured skeletal muscle and participate in muscle regeneration. Biochem Biophys Res Commun 2004, 321:1050–1061
22. Itoh T, Ikeda T, Gomi H, Nakao S, Suzuki T, Itohara S: Unaltered secretion of β-amyloid precursor protein in gelatinase A (matrix metalloproteinase 2)-deficient mice. J Biol Chem 1997, 272:22389–22392
23. Fukada S, Higuchi S, Segawa M, Koda K, Yamamoto Y, Tsujikawa K, Kohama Y, Uezumi A, Imamura M, Miyagoe-Suzuki Y, Takeda S, Yamamoto H: Purification and cell-surface marker characterization of quiescent satellite cells from murine skeletal muscle by a novel monoclonal antibody. Exp Cell Res 2004, 296:245–255
24. Kitamura T, Koshino Y, Shibata F, Oki T, Nakajima H, Nosaka T, Kumagai H: Retrovirus-mediated gene transfer and expression cloning: powerful tools in functional genomics. Exp Hematol 2003, 31:1007–1014
25. Morita S, Kojima T, Kitamura T: Plat-E: an efficient and stable system for transient packaging of retroviruses. Gene Ther 2000, 7:1063–1066
26. Lee SJ, McPherron AC: Regulation of myostatin activity and muscle growth. Proc Natl Acad Sci USA 2001, 98:9306–9311
27. Holly J, Perks C: The role of insulin-like growth factor binding proteins. Neuroendocrinology 2006, 83:154–160
28. Sakamoto K, Yamaguchi S, Ando R, Miyawaki A, Kabasawa Y, Takagi M, Li CL, Perbal B, Katsube K: The nephroblastoma overexpressed gene (NOV/ccn3) protein associates with Notch1 extracellular domain and inhibits myoblast differentiation via Notch signaling pathway. J Biol Chem 2002, 277:29399–29405
29. Lawler J: The functions of thrombospondin-1 and-2. Curr Opin Cell Biol 2000, 12:634–640
30. Tocharus J, Tsuchiya A, Kajikawa M. Ueta Y, Oka C, Kawaichi M: Developmentally regulated expression of mouse HtrA3 and its role as an inhibitor of TGF-beta signaling. Dev Growth Differ 2004, 46:257–274
31. Colarossi C, Chen Y, Obata H, Jurukovski V, Fontana L, Dabovic B, Rifkin DB: Lung alveolar septation defects in Ltbp-3-null mice. Am J Pathol 2005, 167:419–428
32. McCawley LJ, Matrisian LM: Matrix metalloproteinases: they're not just for matrix anymore! Curr Opin Cell Biol 2001, 13:534–540
33. Balcerzak D, Querengesser L, Dixon WT, Baracos VE: Coordinate expression of matrix-degrading proteinases and their activators and inhibitors in bovine skeletal muscle. J Anim Sci 2001, 79:94–107
34. Kayagaki N, Kawasaki A, Ebata T, Ohmoto H, Ikeda S, Inoue S, Yoshino K, Okumura K, Yagita H: Metalloproteinase-mediated release of human Fas ligand. J Exp Med 1995, 182:1777–1783
35. Lanzrein M, Garred O, Olsnes S, Sandvig K: Diphtheria toxin endocytosis and membrane translocation are dependent on the intact membrane-anchored receptor (HB-EGF precursor): studies on the cell-associated receptor cleaved by a metalloprotease in phorbol-ester-treated cells. Biochem J 1995, 310:285–289
36. Couch CB, Strittmatter WJ: Rat myoblast fusion requires metalloendoprotease activity. Cell 1983, 32:257–265

37. Ohtake Y, Tojo H, Seiki M: Multifunctional roles of MT1-MMP in myofiber formation and morphostatic maintenance of skeletal muscle. J Cell Sci 2006, 119:3822–3832
38. Kherif S, Lafuma C, Dehaupas M, Lachkar S, Fournier JG, Verdière-Sahuqué M, Fardeau M, Alameddine HS: Expression of matrix metalloproteinases 2 and 9 in regenerating skeletal muscle: a study in experimentally injured and mdx muscles. Dev Biol 1999, 205:158–170
39. Fukushima K, Nakamura A, Ueda H, Yuasa K, Yoshida K, Takeda S, Ikeda S: Activation and localization of matrix metalloproteinase-2 and -9 in the skeletal muscle of the muscular dystrophy dog (CXMDJ). BMC Musculoskelet Disord 2007, 8:54
40. von Moers A, Zwirner A, Reinhold A, Brückmann O, van Landeghem F, Stoltenburg-Didinger G, Schuppan D, Herbst H, Schuelke M: Increased mRNA expression of tissue inhibitors of metalloproteinase-1 and -2 in Duchenne muscular dystrophy. Acta Neuropathol (Berl) 2005, 109:285–293
41. Pittenger MF, Mackay AM, Beck SC, Jaiswal RK, Douglas R, Mosca JD, Moorman MA, Simonetti DW, Craig S, Marshak DR: Multilineage potential of adult human mesenchymal stem cells. Science 1999, 284:143–147
42. Conget PA, Minguell JJ: Phenotypical and functional properties of human bone marrow mesenchymal progenitor cells. J Cell Physiol 1999, 181:67–73
43. Caplan AI, Dennis JE: Mesenchymal stem cells as trophic mediators. J Cell Biochem 2006, 98:1076–1084
44. Oh J, Takahashi R, Adachi E, Kondo S, Kuratomi S, Noma A, Alexander DB, Motoda H, Okada A, Seiki M, Itoh T, Itohara S, Takahashi C, Noda M: Mutations in two matrix metalloproteinase genes, MMP-2 and MT1-MMP, are synthetic lethal in mice. Oncogene 2004, 23: 5041–5048
45. El Fahime E, Torrente Y, Caron NJ, Bresolin MD, Tremblay JP: In vivo migration of transplanted myoblasts requires matrix metalloproteinase activity. Exp Cell Res 2000, 258:279–287
46. Gearing AJ, Beckett P, Christodoulou M, Churchill M, Clements J, Davidson AH, Drummond AH, Galloway WA, Gilbert R, Gordon JL, Leber TM, Mangan M, Miller K, Nayee P, Owen K, Patel S, Thomas W, Wells G, Wood LM, Woolley K: Processing of tumour necrosis factor-alpha precursor by metalloproteinases. Nature 1994, 370: 555–557

Acta Myologica • 2008; XXVII; p. 30-36

Vasodilation of intramuscular arterioles under shear stress in dystrophin-deficient skeletal muscle is impaired through decreased nNOS expression

K. Sato[1,2,3], T. Yokota[1], S. Ichioka[4], M. Shibata[5], S. Takeda[1]

[1] Department of Molecular Therapy, National Institute of Neuroscience, National Center of Neurology and Psychiatry, Kodaira, Tokyo 187-8502, Japan; [2] Cellport Clinic Yokohama, Minami-nakadori 3-35, Naka-ku, Yokohama, Kanagawa, 231-0006, Japan; [3] Department of Plastic and Reconstructive Surgery, Graduate School of Medicine, The University of Tokyo, Bunkyo-ku, Tokyo 113-0033, Japan; [4] Department of Plastic and Reconstructive Surgery, Saitama Medical School, Moroyama, Iruma-gun, Saitama 350-0451, Japan; [5] Department of Biomedical Engineering, Graduate School of Medicine, The University of Tokyo, Bunkyo-ku, Tokyo 113-0033, Japan

Duchenne muscular dystrophy (DMD) is a lethal X-linked disorder of striated muscle caused by the absence of dystrophin. Recently, impairment of vascular dilation under shear stress has been found in DMD, but the underlying molecular mechanism is not fully understood. Moreover, dilation of intramuscular arterioles, which may be a key to the molecular pathogenesis, has not been addressed yet. We examined dilation of arterioles in the mouse cremaster muscle under shear stress due to ligation. The vasodilation was significantly impaired in dystrophin-deficient *mdx* mice as well as in neuronal nitric oxide synthase (nNOS)-deficient mice; however, neither endothelial NOS-deficient mice nor α1-syntrophin-deficient mice showed any difference in vasodilation from control mice. These results indicate that nNOS is the main supplier of nitric oxide in shear stress-induced vasodilation in skeletal muscle, but that the sarcolemmal localization of nNOS is not indispensable for the function. In contrast, the response to acetylcholine or sodium nitroprusside was not impaired in *mdx* or nNOS-deficient mice, suggesting that pharmacological treatment using a vasoactive agent may ameliorate skeletal and cardiac muscle symptoms of DMD.

Key words: Duchenne muscular dystrophy, blood flow, dystrophin, nitric oxide synthase, vasodilation

Introduction

Nitric oxide (NO) is a vasoactive agent generated by nitric oxide synthase (NOS). Neuronal NOS (nNOS) is highly expressed in skeletal muscle compared with endothelial NOS (eNOS) and inducible NOS (iNOS). nNOS is anchored by α1-syntrophin, a member of the dystrophin-glycoprotein complex (DGC), at the sarcolemma in skeletal muscle (1-6). Dystrophin is a cytoskeletal protein, and its absence together with the secondary loss of DGC from the sarcolemma is responsible for Duchenne muscular dystrophy (DMD), a severe muscle disease characterized by progressive skeletal muscle degeneration complicated with cardiomyopathy (5). nNOS expression is greatly reduced at the mRNA level in dystrophin-deficient muscle (2). Moreover, the attenuation of α-adrenergic vasoconstriction is impaired in contracting dystrophin-deficient muscle, suggesting that nNOS has a specific role in protection from sympathetic vasoconstriction (7, 8). In addition, the localization of nNOS at the sarcolemma through α1-syntrophin is indispensable for the attenuation of α-adrenergic vasoconstriction during muscle contraction (9). Recently, Loufrani et al. showed that the carotid and mesenteric arteries of *mdx* mice, an animal model of DMD, do not dilate properly under shear stress, although they are dilated normally by treatment with either an NOS stimulator, such as acetylcholine (ACh), or an NO donor, such as sodium nitroprusside (SNP) (10). They concluded that the endothelial dystrophin plays an invaluable role in vasodilation under shear stress. In addition, the molecular background is not clearly understood, although flow-induced remodeling in arterial wall is deficient in *mdx* mice when stimulated by arterial ligation or hydralazine (11, 12). To clarify the role of nNOS in intramuscular arterioles in vivo, we studied vasodilation in the mouse cremaster muscle. We caused the modified parallel occlusion of arterioles by microsurgical nylon thread ligation (13-16). We enlisted the participation of DGC in shear-stress vasodilation by using *mdx* mice. We also determined the significance of the localization of nNOS at the sarcolemma by using α1-

Address for correspondence: S. Takeda, Department of Molecular Therapy, National Institute of Neuroscience, National Center of Neurology and Psychiatry, 4-1-1 Ogawa-higashi, Kodaira, Tokyo 187-8502, Japan. Fax +81 42 3461750. E-mail: takeda@ncnp.go.jp

syntrophin knockout mice (α1syn$^{-/-}$). In addition, we used nNOS knockout (nNOS$^{-/-}$) and eNOS knockout (eNOS$^{-/-}$) mice to clarify which NOS is involved in vasodilation under shear stress.

Materials and methods

Animals

Mdx mice and their controls, C57Bl/10 mice (B10), α1syn$^{-/-}$ mice generated in C57Bl/6 mice (B6), and their wild-type littermates (α1syn$^{+/+}$), aged 8-10 weeks were used (17). Eight- to 10-week-old nNOS$^{-/-}$ and eNOS$^{-/-}$ mice (B6 background) were supplied by the Jackson Laboratory. They were anesthetized by intraperitoneal injection of 1.2×10^{-3} g carbamic acid ethyl ester per gram of body weight. At the end of the experiment, animals were sacrificed by an overdose of pentobarbital. All protocols were approved by the Institutional Animal Care and Use Committee of the National Institute of Neuroscience and were performed in compliance with the Guide for the Care and Use of Division of Laboratory Animal Resources.

Experimental Design

We mounted and fixed mouse on experimental stage under anesthesia and scrotum of each mouse was placed on a clear silicone dish as shown in Figure 1a. The cremaster muscle was exposed as described with minor modification (18), and was observed under an intravital microscope at 450 magnifications. The exposed cremaster muscle was deoxygenated by continuous superfusion (5 ml/min) of buffered Tyrode solution (34 ± 0.5 °C, pH 7.35-7.45) bubbled with 95% N_2 and 5% CO_2 gas. Captured microcirculatory images were converted to digital images by the computer and recorded by VTR (Fig. 1a). To calculate the shear stress, we used CapiFlow® (IM-Capiflow, Kista, Sweden), a fully computerized system for the measurement of red blood cell velocity, as previously described (19, 20).

Drug treatment

We first examined the vasodilatory response of third-order arterioles (A3; about 20 μm) in mouse cremaster muscles (Fig. 1b) (22). ACh or SNP was added to the buffer solution and applied directly to the muscle, based on previous reports with modification (23, 24). The vessel diameter was measured before and just after drug administration and the dilatory ratio was calculated as: diameter of arteriole after drug treatment/ before drug treatment. To determine adequate dose, ACh or SNP was exposed from its lower concentration to higher concentration. Before increasing dose, we waited for maximum ten minutes until no more dilatory effect was observed by previous dose. Papaverin was added at the final part of experiments to know the extent of maximum dilation of vessels. We also examined the effect of NO synthesis inhibition by adding N-omega-nitro-L-arginine methyl ester (L-NAME, 0.1 mmol/L) to the buffer from 10 minutes before ACh or SNP administration.

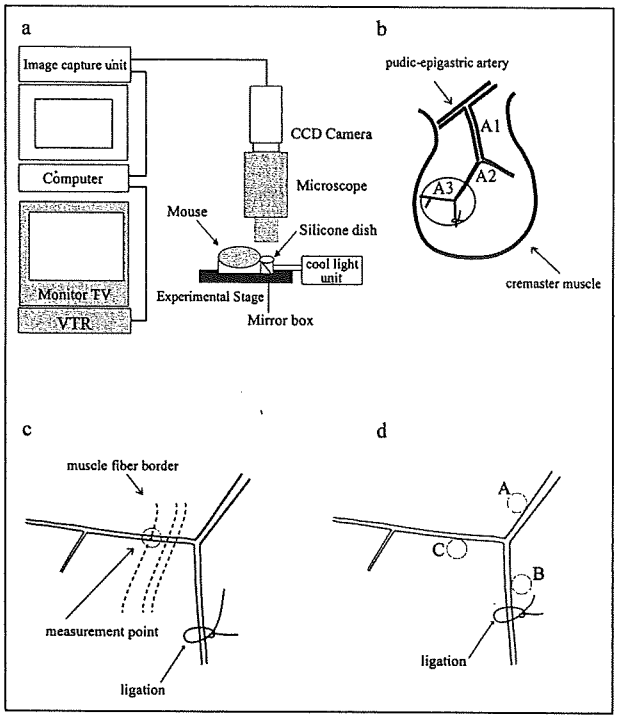

Figure 1. Observation and measurement of dilation of intramuscular arterioles induced by drug treatment or by shear stress in mouse cremaster muscle. (a) Optical system consisting of a cool light unit, mirror box, 450X intravital microscope (MZFL3, Leica Microsystems, Heidelberg, Germany), cooled, color 3 charge-coupled device (CCD) camera, image capture unit (C5810, Hamamatsu Photonics K.K., Hamamatsu, Japan), computer (Apple Macintosh G4, Apple, Cupertino, California), and video cassette recorder (HR-STG300, Victor JVC, Yokohama, JAPAN). (b) Arterioles in the mouse cremaster muscle are classified as indicated. A1; first-order arterioles, A2; second-order arterioles, A3; third-order arterioles. Observation area was indicated by circle. (c) Measurements of arteriole diameter were performed 120-1000 μm from the point of divergence, and the observation point was decided in reference to the border of muscle fibers. (d). Points for measurements of tissue pO_2 during parallel occlusion in A3 area: A, around the main arteriole; B, around the ligation site; and C, the original point for measurements of dilation of arterioles.

Shear stress

We used parallel occlusion method to increase the blood flow velocity in nonoccluded parallel arteriolar branches in vivo, based on the previous studies (13-16). The arteriole was ligated using 10-0 nylon thread with needle to produce shear stress (Fig. 1c) (13). The ligated portion and the measured point (A3) were remote enough from the branching point to avoid artifactual effects. The dilatory ratio for shear stress experiments was calculated as: diameter of arteriole after ligation/ before ligation. The dilatory ratio was also examined under indomethacin ($1.0x10^{-3}$, $5.0x10^{-2}$, $1.0x10^{-2}$ or 0.5 mmol/L) administration, when Prostaglandin I_2 (PGI_2) ($1.0x10^{-4}$ mmol/L) was added to the buffer solution or we induced vasodilation by parallel occlusion. L-NAME and indomethacin were supplied from 10 minutes before ligation. Without L-NAME treatment, shear stress-induced vasodilation was observed for a longer period as long as 20 minutes in 4 B10 and 4 *mdx* mice.

Measurements of partial pressure of oxygen (pO_2)

Observations of the microcirculation and in vivo partial pressure of oxygen (pO_2) measurements were made with a microscope and the oxygen-dependent quenching of phosphorescence decay technique, as previously described (21). We measured tissue pO_2 of B10 (n = 3) and *mdx* mice (n = 3) at three distinct points of cremaster muscles before and after ligation by the phosphorescence quenching method (Fig. 1d).

Histological analysis and immunohistochemistry

Ten-micrometer cryosections of cremaster muscles were prepared, air-dried, and stained with hematoxylin and eosin (H&E). Six-micrometer acetone-fixed cryosections were prepared, blocked with goat serum, and then incubated with primary antibodies, rabbit against nNOS (Zymed Laboratories) and rat against CD31/PECAM-1 (Southern Biotechnology Associates) at room air temperature. Alexa 488-labeled goat anti-rabbit IgG (H + L) (Molecular Probes) and Alexa 594-labeled goat anti-rat IgG (H + L) were used as the secondary antibody. The sections were viewed and photographed by a laser microscope, TCSSP™ (Leica Microsystems).

Statistical analysis

Results were expressed as means ± standard error of the mean (SEM). Results were compared between *mdx* mice and B10, α1syn$^{-/-}$ and α1syn$^{+/+}$ mice, and eNOS$^{-/-}$ or nNOS$^{-/-}$ mice and B6. The effect of L-NAME pretreatment was also evaluated. The significance of the differences between groups was determined by Mann-Whitney U test or ANOVA. Values of $p < 0.05$ were considered to be significant.

Results

Drug induced vasodilation

Maximum arteriolar dilation was determined for administration of ACh or SNP, and then compared with the dilation by the treatment with 1.0 mmol/L of Papaverine. The optimal dose of both ACh and SNP was 1.0 mmol/L for maximum dilatory ratio (Fig. 2) and the dose was used for subsequent examinations (Fig. 3).

The administration of ACh or SNP gave almost the same dilatory ratio between B10 (n = 7) and *mdx* mice (n = 7), α1syn$^{+/+}$ (n = 5) and α1syn$^{-/-}$ (n = 5) and, eNOS$^{-/-}$ (n = 4) or nNOS$^{-/-}$ mice (n = 4) and B6 (n = 4) (Figs. 3a and 3b). This result does not conflict with the conclusion of a previous study using nNOS- and eNOS-deficient mice that expression of either nNOS or eNOS is sufficient for ACh-induced dilation (25). Pretreatment of L-NAME gave the same degree of inhibition in ACh-induced vasodilation in B10 (n = 5) and in *mdx* mice (n = 5), but did not significantly alter the dilatory ratio in SNP-induced vasodilation in these mice.

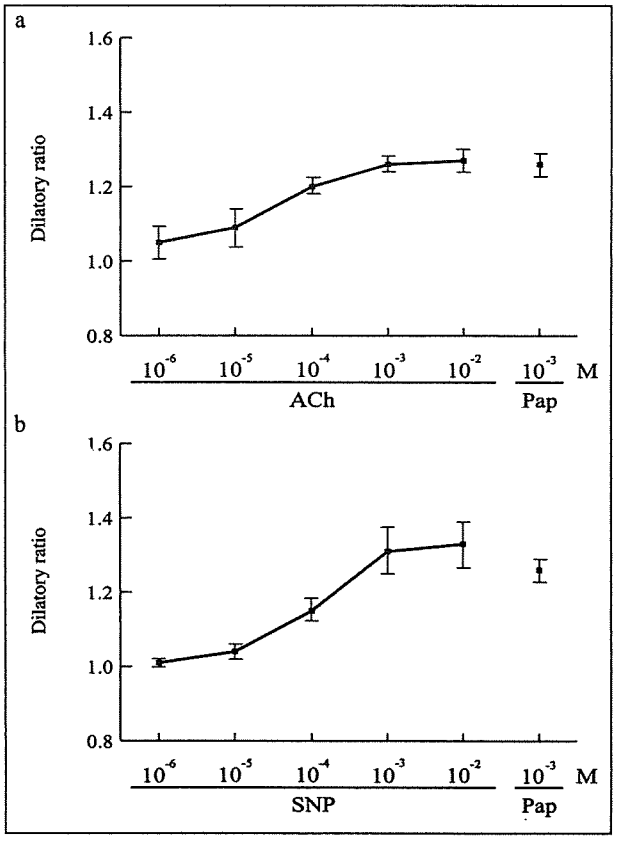

Figure 2. Responses of arterioles for vasodilatory agents, ACh and SNP in three B10. Graphs are showing dilatory ratio against various doses of ACh (a) or SNP (b), in reference to maximum dilation by treatment of 10^{-3} M of Papaverin (Pap).

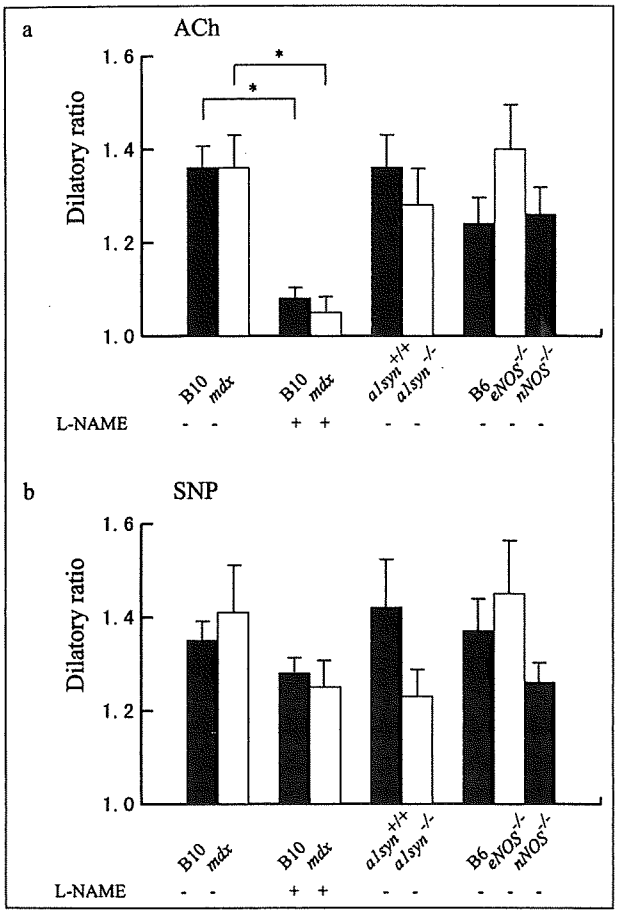

Figure 3. Effects of vasodilative agents on dilation of mouse cremaster arterioles of B10 (black bar), mdx (white bar), B10 pretreated with L-NAME (black bar), mdx pretreated with L-NAME (white bar), α1syn$^{+/+}$ (black bar), α1syn$^{-/-}$ (white bar), B6 (black bar), eNOS$^{-/-}$ (white bar), and nNOS$^{-/-}$ (black bar) mice. (a) After pretreatment with L-NAME, ACh-induced vasodilation was reduced both in B10 and in mdx mice. Values are indicated as mean ± SEM. Asterisk (*) shows statistical significance ($p < 0.05$). (b) Vasodilation induced by SNP was not statistically significant between the mice we examined.

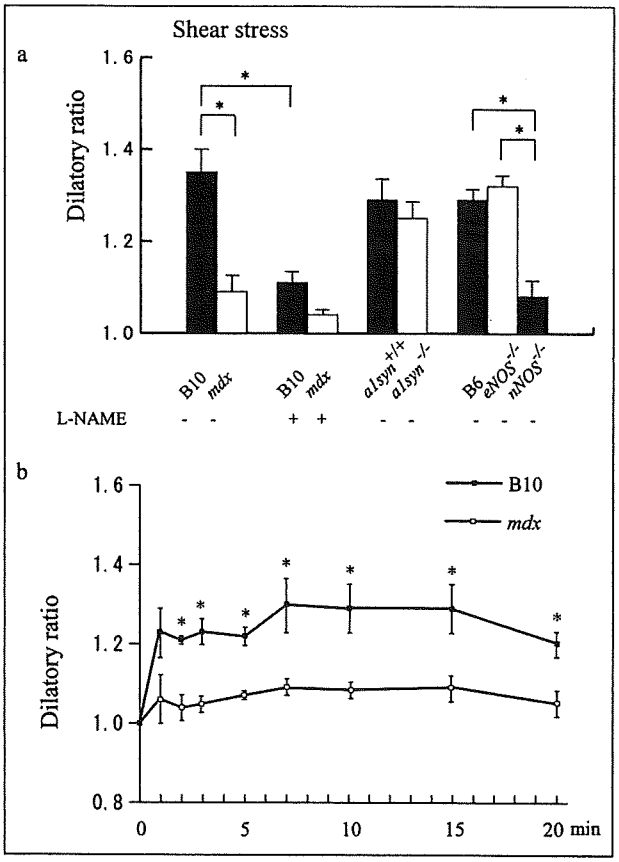

Figure 4. Effects of shear stress-induced dilation of mouse cremaster arterioles of B10 (black bar), mdx (white bar), B10 pretreated with L-NAME (black bar), mdx pretreated with L-NAME (white bar), α1syn$^{+/+}$ (black bar), α1syn$^{-/-}$ (white bar), B6 (black bar), eNOS$^{-/-}$ (white bar), and nNOS$^{-/-}$ (black bar) mice. (a) mdx mice, B10 pretreated with L-NAME, mdx mice pretreated with L-NAME and nNOS$^{-/-}$ mice showed impaired vasodilation under shear stress. (b) Extended observation of shear stress-induced vasodilation. The vessel diameter in B10 rapidly increased after vessel ligation and reached a stable level within 10 minutes (n = 4). The dilation of arterioles was severely impaired in mdx mice (n = 4). The difference between mdx mice and B10 was observed as long as 20 minutes after the ligation.

Shear stress-induced vasodilation

In contrast, shear stress-induced vasodilation was significantly impaired in *mdx* mice (n = 10) compared with that of B10 (n = 10) (Fig. 4a), and in addition, the calculated shear stresses were different (Table 1). Interestingly, although nNOS$^{-/-}$ mice (n = 5) showed impaired vasodilation, eNOS$^{-/-}$ mice (n = 5) did not show significant differences in the dilatory ratio when compared with that of B6 (n = 5), indicating that nNOS is the main supplier of NO in the shear stress-induced vasodilation of arterioles in skeletal muscle. On the other hand, α1syn$^{-/-}$ mice (n = 5) did not show significant differences in the dilation compared with the control α1syn$^{+/+}$ mice (n = 5), suggesting that the intramuscular localization of nNOS at the sarcolemma is not critical for shear stress-induced vasodilation. After pre-treatment with L-NAME, shear stress-induced vasodilation was significantly decreased in B10 (n = 5).

As shown in Figure 4b, under a longer observation of shear stress-induced vasodilation in the absence of L-NAME, the difference between *mdx* mice and B10 was still observed at least 20 minutes after the ligation.

Table 1. Relationship of vasodilation and shear stress in mouse cremaster arterioles.

	Blood cell velocity (cm/s)		Diameter (μm)		Shear stress rate
	before ligation	after ligation	before ligation	after ligation	
B10 (n = 3)	0.48 ± 0.05	0.67 ± 0.20	18.7 ± 0.9	24.2 ± 0.2	1.02 ± 0.16
mdx (n = 3)	0.41 ± 0.05	0.91 ± 0.23*	18.8 ± 0.7	19.8 ± 0.1*	2.02 ± 0.23*

Shear stress rates were calculated as (shear stress before ligation) / (shear stress after ligation). Values are expressed as mean ± S.E.M. * = $p < 0.05$

PGI_2 induced vasodilation

There were significant differences between shear stress-induced and PGI_2-induced vasodilation in dilatory ratios against high concentrations of indomethacin in B10 (Fig. 5). These data indicated that high concentration of indomethacin treatment could completely antagonize PGI_2-induced vasodilation, but the treatment cannot completely inhibit shear stress-induced vasodilation.

Alternation of pO_2 before and after ligation

There were no significant differences in tissue pO_2 levels between before and after ligation not only in B10 but also in *mdx* mice (Fig. 6).

Immunohistochemical observation of NOS expression

In H&E stained tissues, centrally nucleated fibers, which represent muscle regeneration, were observed in only *mdx* mice (Figs. 7a-e). The immunohistochemical analysis showed that nNOS was observed mainly at the sarcolemma rather than in the endothelium and vascular smooth muscle in B10 and $eNOS^{-/-}$ mice (Figs. 7b and 7h). In $\alpha 1syn^{-/-}$ mice, nNOS was not localized at the sarcolemma but remained in the cytoplasm (Fig. 7f), as previously reported (14, 26). Less nNOS was found in *mdx* mice, and it was not detected in $nNOS^{-/-}$ mice (Figs. 7d and 7j).

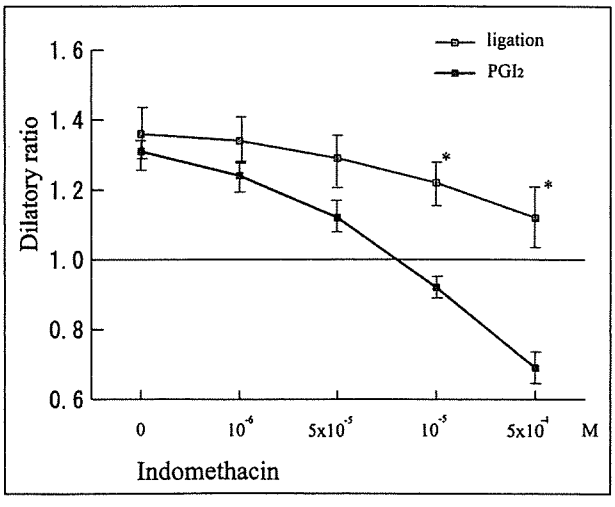

Figure 5. Under various dose of indomethacin, vasodilation was induced either by treatment of Prostaglandin I_2 (PGI_2) or by parallel occlusion (ligation) in B10 cremaster muscle arterioles (n = 5).

Discussion

Nitric oxide is one of the most important factors in shear stress-induced vasodilation especially by parallel occlusion method (10, 14, 27). Other factors, such as prostaglandins, were reported to contribute to shear stress-induced dilation in various models (15, 16, 28), but we showed that indomethacin, an inhibitor of prostaglandins, did not prevent the increase in diameter in shear stress condition. In addition, we concluded that the parallel occlusion method did not cause tissue hypoxia or acute ischemia. Thus, we demonstrated that dilation of arterioles in the mouse cremaster muscle under shear stress by the parallel occlusion method depends mainly on NO, especially that produced by nNOS. In particular, *mdx* and $nNOS^{-/-}$ mice showed impaired vasodilation in parallel occlusion,

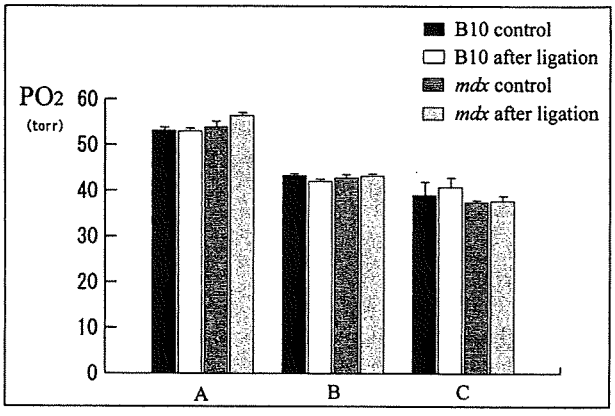

Figure 6. Histogram showing pO_2 at the observation points. There are no significant differences in alterations of tissue pO_2 during parallel occlusion.

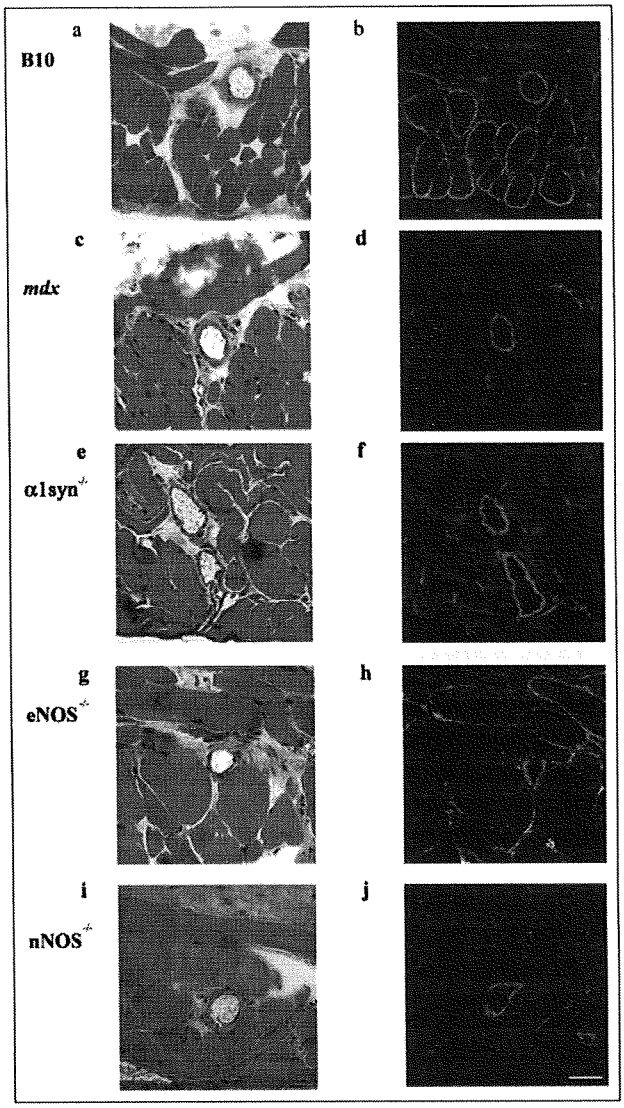

Figure 7. nNOS expression and localization in vascular endothelium and cremaster muscles of mice. H&E (a, c, e, g, and i) and double staining with nNOS (green) and PECAM-1 (red) antibodies (b, d, f, h, and i) of B10 (a, b), mdx (c, d), α1syn$^{-/-}$ (e, f), eNOS$^{-/-}$ (g, h), and nNOS$^{-/-}$ (i, j) mice. Centrally located nuclei, a typical feature of regenerated muscle, are found only in mdx mice (c). In B10 and eNOS$^{-/-}$ cremaster muscles, nNOS expression was observed at the sarcolemma. In contrast, the expression was greatly reduced or not detected in mdx or nNOS$^{-/-}$ mice, respectively. Bar, 40 μm.

whereas responses to ACh and SNP were unaltered. Decreased expression of nNOS in *mdx* skeletal muscle may be important as a cause of this finding.

It is intriguing to know the relationship between shear stress-induced vasodilation and the localization of nNOS. Koller et al. showed that shear stress-induced vasodilation of 80- to 156-μm arterioles was inhibited by removal of the endothelium or by addition of indomethacin in rat cremaster muscle, but they did not identify the responsible molecules of vascular dilation (29). In our study, nNOS expression was mainly found in the sarcolemma and less frequently in the endothelium or vascular smooth muscle, implying that skeletal muscle nNOS is possibly involved in dilation of intramuscular arterioles at the very end of the skeletal muscle circulation under shear stress. nNOS is anchored to the sarcolemma through α1-syntrophin. α1syn$^{-/-}$ mice showed altered distribution of nNOS expression in cytoplasm, but showed no significant differences in shear stress-induced vasodilation between α1syn$^{-/-}$ mice and α1syn$^{+/+}$ mice. Thus, the sarcolemmal localization of nNOS through expression of α1-syntrophin is not indispensable for vasodilation. However, how dystrophin or other molecules transduce mechanostress to soluble nNOS is unresolved (6). The defective vasodilation under shear stress due to nNOS deficiency in *mdx* mice might be related to its muscle degradation (14).

It is very interesting to note the amelioration of dystrophic phenotypes in nNOS transgenic *mdx* mice, although the localization of nNOS cannot have been improved (30). Decreased vasodilation just after muscle contraction has also been demonstrated in *mdx* skeletal muscle (31). Leinonen et al. found that capillary circulation in skeletal muscle was impaired in DMD (32), and deteriorated attenuation of α-adrenergic vasoconstriction during exercise may participate in this pathophysiology (7). Moreover, blood flow must be increased to accommodate the augmented metabolic demands of the muscle, not only in exercise. Intramuscular arterioles in *mdx* mice cannot afford to respond to the increased demands, and their failure may result in relative ischemia in the skeletal muscle and cardiac phenotypes of dystrophin deficiency. Asai et al. very recently showed that the functional ischemia in contraction-induced myofibers in *mdx* mice is due to nNOS deficiency and indicated that vasoactive drugs may ameliorate muscle damage (33). Even in dystrophin-deficient skeletal muscle, cholinergic vascular modulation was well preserved. Therefore, our study indicates that pharmacological treatment using a vasoactive agent is applicable to at least skeletal muscle symptoms in patients suffering from DMD.

In conclusion, we demonstrated that vasodilation of intramuscular arterioles under shear stress was impaired in dystrophin-deficient *mdx* mice. This impairment may be related to phenotypes of DMD, not only in skeletal muscle but also in cardiac muscle.

Acknowledgements

This work was supported by Grants-in-Aid from the Human Frontier Science Program, Scientific Research for

Center of Excellence, Research on Nervous and Mental Disorders (10B-1, 13B-1), Health Science Research Grants for Research on the Human Genome and Gene Therapy (H10-genome-015, H13-genome-001) and for Research on Brain Science (H12-brain-028) from the Ministry of Health, Labor, and Welfare of Japan, Grants-in-Aid for Scientific Research (10557065, 11470153, 11170264, 14657158, and 15390281) from the Ministry of Education, Culture, Sports, Science, and Technology for Japan, and a Research Grant from the Human Frontier Science Project. This work was also carried out as a part of the "Ground-based Research Announcement for Space Utilization" promoted by the Japan Space Forum. T. Yokota is a Research Fellow of the Japan Society for the Promotion of Science (JSPS).

References

1. Brenman JE, Chao DS, Xia H, et al. Nitric oxide synthase complexed with dystrophin and absent from skeletal muscle sarcolemma in Duchenne muscular dystrophy. Cell 1995;82:743-52.
2. Chang W, Iannaccone ST, Lau KS, et al. Neuronal nitric oxide synthase and dystrophin-deficient muscular dystrophy. Proc Nat Acad Sci USA 1996;93:9142-7.
3. Brenman JE, Chao DS, Gee SH, et al. Interaction of nitric oxide synthase with the postsynaptic density protein PSD-95 and α1-syntrophin mediated by PDZ domains. Cell 1996;84:757-67.
4. Yokota T, Miyagoe Y, Hosaka Y, et al. Aquaporin-4 is absent at the sarcolemma and at perivascular astrocyte endfeet in α1-syntrophin knockout mice. Proc Japan Acad 2000;76B:22-7.
5. Hoffman EP, Brown RH Jr, Kunkel LM. Dystrophin: the protein product of the Duchenne muscular dystrophy locus. Cell 1987;51:919-28.
6. Suzuki N, Motohashi N, Uezumi A, et al. NO production results in suspension induced muscle atrophy through dislocation of neuronal NOS. J Clin Invest 2007;117:2468-76.
7. Thomas GD, Sander M, Lau KS, et al. Impaired metabolic modulation of α-adrenergic vasoconstriction in dystrophin-deficient skeletal muscle. Proc Natl Acad Sci USA 1998;95:15090-5.
8. Fadel PJ, Zhao W, Thomas GD. Impaired vasomodulation is associated with reduced neuronal nitric oxide synthase in skeletal muscle of ovariectomized rats. J Physiol 2003;549:243-53.
9. Thomas GD, Shaul PW, Yuhanna IS, et al. Vasomodulation by skeletal muscle-derived nitric oxide requires α-syntrophin-mediated sarcolemmal localization of neuronal nitric oxide synthase. Circ Res 2003;92:554-60.
10. Loufrani L, Matrougui K, Gorny D, et al. Flow (shear stress)-induced endothelium-dependent dilation is altered in mice lacking the gene encoding for dystrophin. Circulation 2001;103:864-70.
11. Loufrani L, Li Z, Levy BI, et al. Excessive microvascular adaptation to chronic changes in blood flow in mice lacking the gene encoding for desmin. Arterioscler Thromb Vasc Biol 2002;22:1579-84.
12. Loufrani L, Henrion D. Vasodilator treatment with hydralazine increases blood flow in *mdx* mice resistance arteries without vascular wall remodeling or endothelium function improvement. J Hyperten 2005;23:1855-60.
13. Koller A, Kaley G. Flow velocity-dependent regulation of microvascular resistance in vivo. Microcirc Endothelium Lymphatics 1989;6:519-29.
14. Koller A, Kaley G. Endothelium regulates skeletal muscle microcirculation by a blood flow velocity-sensing mechanism. Am J Physiol 1990;258:H862-8.
15. Koller A, Kaley G. Prostaglandins mediate arteriolar dilation to increased blood flow velocity in skeletal muscle microcirculation. Circ Res 1990;67:529-34.
16. Frisbee JC, Stepp DW. Impaired NO-dependent dilation of skeletal muscle arterioles in hypertensive diabetic obese Zucker rats. Am J Physio. Heart Circ Physiol 2001;281:H1304-11.
17. Kameya S, Miyagoe Y, Nonaka I, et al. α1-Syntrophin gene disruption results in the absence of neuronal-type nitric-oxide synthase at the sarcolemma but does not induce muscle degeneration. J Biol Chem 1999;274:2193-200.
18. Baez S. An open cremaster muscle preparation for the study of blood vessels in vivo. Microscopy Microvasc Res 1973;5:384-94.
19. Fagrell B, Rosen L, Eriksson SE. Computerized data analysis of capillary blood cell velocity in humans. Int J Microcirc Clin Exp 1994;14:133-8.
20. Bongard O, Fagrell B. Discrepancies between total and nutritional skin microcirculation in patients with peripheral arterial occlusive disease (PAOD). Vasa 1999;19:105-11.
21. Shibata M, Ichioka S, Ando J, et al. Microvascular and interstitial PO(2) measurements in rat skeletal muscle by phosphorescence quenching. Appl Physiol 2001;91:321-7.
22. Kaul DK, Fabry ME, Costantini F, et al. In vivo demonstration of red cell-endothelial interaction, sickling and altered microvascular response to oxygen in the sickle transgenic mouse. J Clin Invest 1995;96:2845-53.
23. Ichioka S, Shibata M, Kosaki K, et al. Effects of shear stress on wound-healing angiogenesis in the rabbit ear chamber. J Surg Res 1997;72:29-35.
24. Ichioka S, Nakatsuka T, Ohura N, et al. Topical application of amrinone (a selective phosphodiesterase III inhibitor) for relief of vasospasm. J Surg Res 2000;93:149-55.
25. Meng W, Ayala C, Waeber C, et al. Neuronal NOS-cGMP-dependent ACh-induced relaxation in pial arterioles of endothelial NOS knockout mice. Am J Physiol 1998;274:H411-5.
26. Miyagoe-Suzuki Y, Takeda S. Association of neuronal nitric oxide synthase (nNOS) with α1-syntrophin at the sarcolemma. Microsc Res Tech 2001;55:164-70.
27. Boegehold MA. Flow-dependent arteriolar dilation in normotensive rats fed low- or high-salt diets. Am J Physiol 1995;269:H1407-14.
28. Sun D, Huang A, Smith CJ, et al. Enhancing release of prostaglandins contributes to flow-induced arteriolar dilation in eNOS knockout mice. Circ Res 1999;85:288-93.
29. Koller A, Sun D, Kaley G. Role of shear stress and endothelial prostaglandins in flow- and viscosity-induced dilation of arterioles in vitro. Circ Res 1993;72:1276-84.
30. Wehling M, Spencer MJ, Tidball JG. A nitric oxide synthase transgene ameliorates muscular dystrophy in *mdx* mice. J Cell Biol 2001;155:123-31.
31. Lau KS, Grange RW, Chang WJ, et al. Skeletal muscle contractions stimulate cGMP formation and attenuate vascular smooth muscle myosin phosphorylation via nitric oxide. FEBS Lett 1998;431:71-4.
32. Leinonen H, Juntunen J, Somer H, et al. Capillary circulation and morphology in Duchenne muscular dystrophy. Eur Neurol 1979;18: H714-21.
33. Asai A, Sahani N, Kaneki M, et al. Primary role of functional ischemia, quantitative evidence for the two-hit mechanism, and phosphodiesterase-5 inhibitor therapy in mouse muscular dystrophy. PLoS ONE 2007;29:e806.

HUMAN GENE THERAPY 19:719–730 (July 2008)

DOI: 10.1089/hum.2007.184

Recombinant Adeno-Associated Virus Type 8-Mediated Extensive Therapeutic Gene Delivery into Skeletal Muscle of α-Sarcoglycan-Deficient Mice

Akiyo Nishiyama,[1] Beryl Nyamekye Ampong,[1] Sachiko Ohshima,[1] Jin-Hong Shin,[1] Hiroyuki Nakai,[2] Michihiro Imamura,[1] Yuko Miyagoe-Suzuki,[1] Takashi Okada,[1] and Shin'ichi Takeda[1]

Abstract

Autosomal recessive limb-girdle muscular dystrophy type 2D (LGMD 2D) is caused by mutations in the α-sarcoglycan gene (α-SG). The absence of α-SG results in the loss of the SG complex at the sarcolemma and compromises the integrity of the sarcolemma. To establish a method for recombinant adeno-associated virus (rAAV)-mediated α-SG gene therapy into α-SG-deficient muscle, we constructed rAAV serotypes 2 and 8 expressing the human α-SG gene under the control of the ubiquitous cytomegalovirus promoter (rAAV2-α-SG and rAAV8-α-SG). We compared the transduction profiles and evaluated the therapeutic effects of a single intramuscular injection of rAAVs into α-SG-deficient ($Sgca^{-/-}$) mice. Four weeks after rAAV2 injection into the tibialis anterior (TA) muscle of 10-day-old $Sgca^{-/-}$ mice, transduction of the α-SG gene was localized to a limited area of the TA muscle. On the other hand, rAAV8-mediated α-SG expression was widely distributed in the hind limb muscle, and persisted for 7 months without inducing cytotoxic and immunological reactions, with a reversal of the muscle pathology and improvement in the contractile force of the $Sgca^{-/-}$ muscle. This extensive rAAV8-mediated α-SG transduction in LGMD 2D model animals paves the way for future clinical application.

Introduction

LIMB-GIRDLE MUSCULAR DYSTROPHY TYPE 2D (LGMD 2D) is caused by mutations in the α-sarcoglycan (α-SG) gene, and is the most frequent cause of the autosomal recessive LGMD. LGMD 2D patients have the clinical characteristics of progressive muscle necrosis in the proximal limb muscles (Eymard *et al.*, 1997). Sarcoglycans (SGs) are essential constituents of the dystrophin-associated protein (DAP) complex, which consists of several membrane-spanning and cytoplasmic proteins, including dystroglycans (α and β), SGs (α, β, γ, and δ), sarcospan, syntrophins (α_1, β_1, and β_2), and dystrobrevins that directly or indirectly associate with dystrophin (Ervasti *et al.*, 1990; Yoshida and Ozawa, 1990; Iwata *et al.*, 1993). A defect in any one of the four SGs can disrupt the entire SG complex. Mutations in four genes encoding α-, β-, γ-, and δ-SG are responsible for autosomal recessive LGMD 2D, 2E, 2C and 2F, respectively (Ervasti *et al.*, 1990; Bonnemann *et al.*, 1995; Noguchi *et al.*, 1995; Nigro *et al.*, 1996; Eymard *et al.*, 1997; Fanin *et al.*, 1997).

Many *in vivo* studies have demonstrated that recombinant adeno-associated virus (rAAV) packaged in various serotypes of AAV capsids exhibits serotype-specific tissue or cell tropism with different transduction efficiencies (Fisher *et al.*, 1997; Greelish *et al.*, 1999; Gao *et al.*, 2002, 2004; Wang *et al.*, 2005). rAAV has been shown to mediate long-term transgene expression in many tissues without evoking severe immune reactions. Some rAAVs efficiently transduce skeletal muscle (Kessler *et al.*, 1996; Xiao *et al.*, 1996; Fisher *et al.*, 1997). rAAV serotype 2 (rAAV2)-mediated muscle gene therapy is a promising approach, but it is effective only locally. In contrast, rAAV serotype 8 (rAAV8)-mediated gene transfer is capable of crossing capillary blood vessels to achieve systemic gene delivery, and effectively transduces genes into cardiac and skeletal muscle (Wang *et al.*, 2005). Therefore, rAAV8 is a good candidate for a therapeutic tool.

To assess the efficacy and therapeutic potential of rAAV8 for LGMD 2D, we directly injected rAAV2-α-SG and rAAV8-α-SG into the tibialis anterior (TA) muscles of 10-day-old α-SG-deficient mice (neonatal $Sgca^{-/-}$ mice). Our data suggested not

[1]Department of Molecular Therapy, National Institute of Neuroscience, National Center of Neurology and Psychiatry, Tokyo 187-8502, Japan.
[2]Department of Molecular Genetics and Biochemistry, University of Pittsburgh School of Medicine, Pittsburgh, PA 15261.

only the extensive expression of α-SG in Sgca$^{-/-}$ skeletal muscle, but also a robust level of expression of α-SG at the sarcolemma after a single intramuscular injection of rAAV8-α-SG. In addition, rAAV8-α-SG effectively transduced the cardiac muscle of 7-week-old Sgca$^{-/-}$ mice (adult Sgca$^{-/-}$ mice). Most importantly, 7 months after the injection of rAAV8-α-SG into neonatal Sgca$^{-/-}$ mice, expression of α-SG and improvement of sarcolemmal function were sustained, without inducing cytotoxic and immunological reactions. Thus, the AAV8 vector is a promising tool for gene therapy of LGMD 2D.

Materials and Methods

Recombinant AAV production

The full-length human α-SG cDNA was amplified from a skeletal muscle single-strand cDNA library (Human Skeletal Muscle Marathon-Ready cDNA; Clontech, Palo Alto, CA) by polymerase chain reaction (PCR) with the following set of oligonucleotide primers: 5′-CTCTGTCACTCACCGGG-3′ (nucleotide positions 2–18) and 5′-AGGATGAAGTC-AGGGCTGGAC-3′ (nucleotide positions 1223–1243) (McNally *et al.*, 1994). The amplification was carried out with LA-Taq polymerase (TaKaRa Bio, Shiga, Japan) for 30 cycles, with each cycle consisting of 94°C for 30 sec and 60°C for 2 min. The PCR products were then cloned into a TA cloning vector (Invitrogen, Carlsbad, CA), and sequenced with an ABI310 sequencer (Applied Biosystems, Foster City, CA). α-SG cDNA was then cloned into an AAV serotype 2 vector plasmid (Xiao *et al.*, 1998; Yuasa *et al.*, 2002) including the cytomegalovirus (CMV) promoter, splicing donor/acceptor (SD/SA) sites derived from the simian virus 40 (SV40), an SV40 poly(A) signal, inverted terminal repeat (ITR) of the AAV2 viral genome, and 2.0 kb of λ DNA, which served as a stuffer (depicted in Fig. 1A).

The vector genome was packaged in the AAV2 capsid or pseudotyped into the AAV8 capsid by triple transfection of

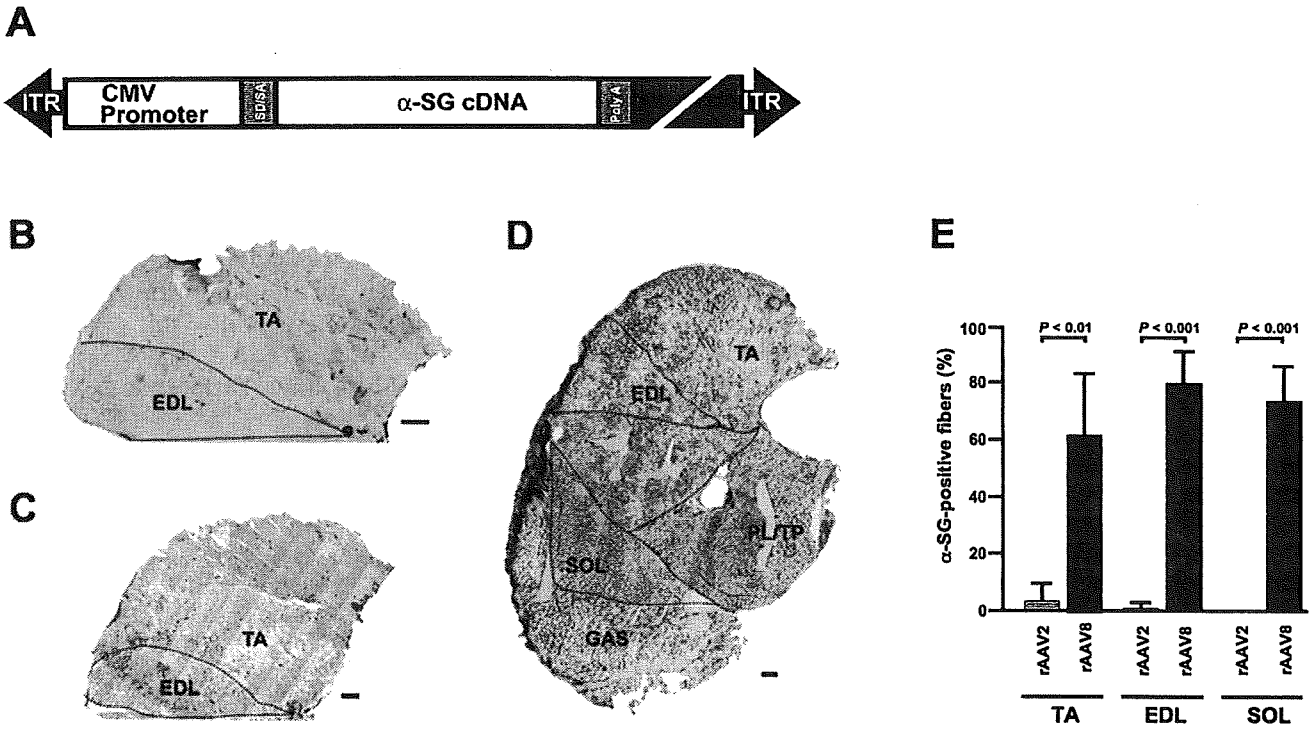

FIG. 1. Widespread expression of α-SG in hind limb muscles after a single injection of rAAV2-α-SG or rAAV8-α-SG into the tibialis anterior (TA) muscles of 10-day-old α-SG-deficient mice. (**A**) Genomic structure of rAAV used in this study. Human α-SG cDNA (1.2 kb) was inserted downstream of the CMV promoter. ITR, inverted terminal repeat from AAV2 genome; SD/SA, splicing donor/acceptor sites derived from SV40 intron; poly(A), a polyadenylation signal from SV40. The large shaded box represents a stuffer sequence derived from λ DNA. (**B–D**) Right TA muscles of neonatal Sgca$^{-/-}$ mice were injected with 1×10^{11} VG of rAAV2-α-SG (**C**) or rAAV8-α-SG (**D**). Four weeks after rAAV injection, the hind limb muscles of Sgca$^{-/-}$ mice were immunolabeled with a rabbit polyclonal antibody to α-SG. Hind limb muscles included the TA, extensor digitorum longus (EDL), plantaris (PL)/tibialis posterior (TP), soleus (SOL), and gastrocnemius (GAS) muscles. The TA and EDL muscles of Sgca$^{-/-}$ mice are shown as negative controls (**B**). Note that α-SG is expressed not only in rAAV8-injected TA muscle, but also in all hind limb muscles after direct injection of rAAV8-α-SG into the right TA muscle (**D**). Scale bars (**B–D**): 500 μm. (**E**) Percentages of α-SG-positive myofibers in TA, EDL, and SOL muscles after injection of rAAV2-α-SG (shaded columns) and rAAV8-α-SG (solid columns) injection into TA muscles of Sgca$^{-/-}$ mice. The right TA muscles of neonatal Sgca$^{-/-}$ mice were transduced with 1×10^{11} VG of rAAV2-α-SG or rAAV8-α-SG. Four weeks after rAAV injection, the hind limb muscles of Sgca$^{-/-}$ mice were immunolabeled with the α-SG antibody and then counterstained with hematoxylin and eosin. Hind limb muscles include the TA, EDL, and SOL muscles. The percentage of α-SG-positive myofibers was calculated on the basis of more than 200 total myofibers in cross-sections from three animals for each group. p Values are indicated and show statistical significance between Sgca$^{-/-}$ mice and rAAV8-injected Sgca$^{-/-}$ mice ($p < 0.01$ for TA, $p < 0.001$ for EDL, and $p < 0.001$ for SOL).

the AAV vector plasmid, AAV helper plasmid (p5E18-VD2/8) (Wang *et al.*, 2005), and adenovirus helper plasmid (XX6) (Xiao *et al.*, 1998) at a molecular ratio of 1:1:1 in 293 cells, using the calcium phosphate coprecipitation method (Wigler *et al.*, 1980). All the vectors were then purified by two cycles of cesium chloride gradient centrifugation, and concentrated as described by Burton and coworkers (1999). The final viral preparations were kept in phosphate-buffered saline. Physical particle titers were determined by a quantitative dot-blot assay.

Administration of rAAV vectors to murine skeletal muscle

All animal-handling procedures were done in accordance with a protocol approved by the committee of the National Institute of Neuroscience (National Center of Neurology and Psychiatry, Kodaira, Japan). Wild-type ($Sgca^{+/+}$) and $Sgca^{-/-}$ mice (Burnham Institute, La Jolla, CA) were used. The TA muscles of 10-day-old (neonate) and 7-week-old (adult) $Sgca^{-/-}$ mice were transduced with 1×10^{11} vector genomes (VG) (10 μl) and 5×10^{11} VG (50 μl), respectively, of rAAV2- or rAAV8-α-SG, using 29-gauge needles.

Transgene expression analyses

Histological and immunohistochemical analyses were performed as described (Imamura *et al.*, 2000; Yuasa *et al.*, 2002). Cryosections (6 μm thick) were prepared from frozen muscle.

For colorimetric immunodetection of α-SG, blocked cryosections were incubated with a 1:1000 dilution of rabbit polyclonal anti-α-SG (Araishi *et al.*, 1999) for 1 hr at room temperature. The signal was visualized with a VECTASTAIN ABC kit (Vector Laboratories, Burlingame, CA) and then counterstained with hematoxylin and eosin (H&E). Stained sections were photographed with a light microscope (Leica, Heidelberg, Germany) using DP70 image scanning software (Olympus, Tokyo, Japan).

For fluorescence immunohistochemical detection of SGs, cryosections were fixed by immersion in cold acetone at –20°C for 5 min. After blocking with 2% casein in Tris-buffered saline (TBS, pH 7.4) at room temperature for 1 hr, α-SG was detected with rabbit polyclonal anti-α-SG (1:1000 dilution) (Araishi *et al.*, 1999). β-, γ-, and δ-SGs were detected with mouse monoclonal anti-β-SG (NCL-b-SARC, 1:50 dilution; Novocastra Laboratories, Newcastle-upon-Tyne, UK), anti-γ-SG (1:50 dilution), and anti-δ-SG (DSG-1; 1:50 dilution), respectively, after blocking with an M.O.M. kit (Vector Laboratories). Mouse monoclonal antibodies against γ-SG and δ-SG (DSG-1) were generated in our laboratory (Yamamoto *et al.*, 1994; Noguchi *et al.*, 1999). The signal was visualized with Alexa 488-conjugated anti-rabbit and anti-mouse IgG antibodies (Invitrogen Molecular Probes, Eugene, OR). Fluorescence signals were observed with a confocal laser-scanning microscope (Leica TCS SP; Leica).

Sodium dodecyl sulfate–polyacrylamide gel electrophoresis (SDS–PAGE) and protein transfer to a polyvinylidene di-

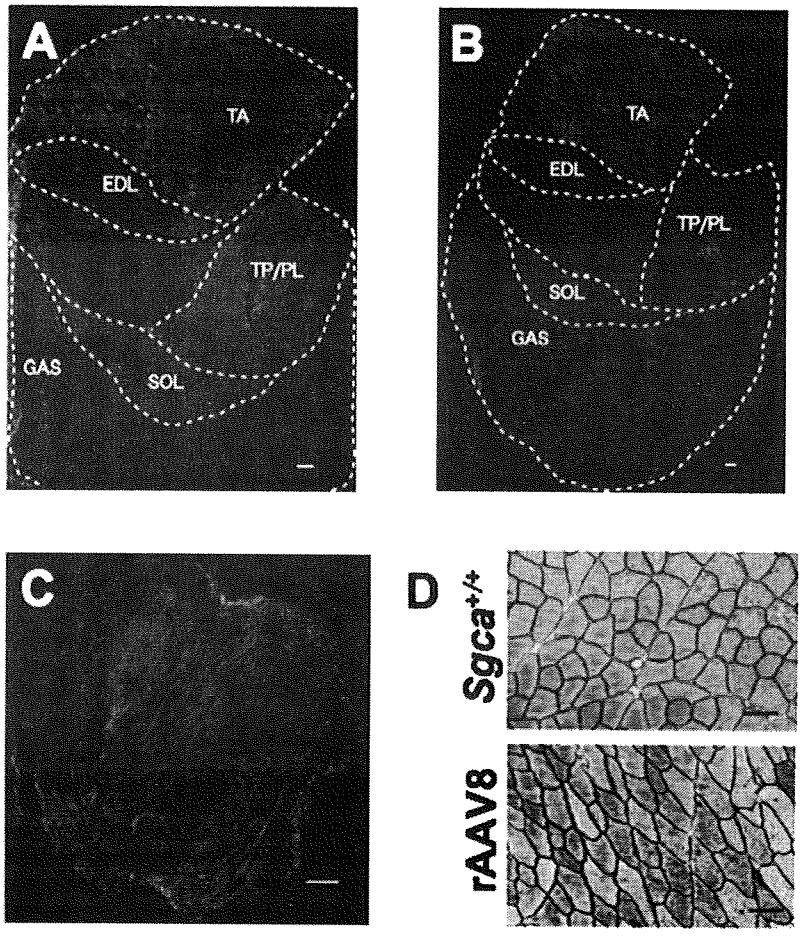

FIG. 2. Extensive α-SG expression after injection of rAAV8-α-SG into TA muscles of 7-week-old α-SG-deficient mice. Right TA muscles of adult $Sgca^{-/-}$ or $Sgca^{+/+}$ mice were transduced with 5×10^{11} VG of rAAV8-α-SG. Four weeks after rAAV8 injection, a cross-section of the right hind limb muscles (rAAV8-injected) (**A**), left contralateral hind limb muscles (**B**), and cardiac apex (**C**) were labeled by indirect immunofluorescence, using α-SG antibody (green). Scale bars: (**A** and **B**) 500 μm; (**C**) 100 μm. Note the widespread expression of α-SG in the hind limb muscles and cardiac muscle of rAAV8-α-SG-injected mice. (**D**) Cross-sections of TA muscle from $Sgca^{+/+}$ and rAAV8-injected $Sgca^{+/+}$ (rAAV8) mice were immunolabeled with α-SG antibody and counterstained with hematoxylin and eosin. Overexpression of α-SG caused no cytotoxic reactions in $Sgca^{+/+}$ muscle. Scale bars (**D**): 50 μm.

fluoride (PVDF) membrane were performed as described by Laemmli (1970) and Kyhse-Andersen (1984), respectively. Protein concentrations were determined with a protein assay kit (Bio-Rad, Hercules, CA) with bovine serum albumin as a standard.

Transgene copy number analyses

Cryosections of mouse hind limb muscle were collected for vector copy number analysis by quantitative PCR. After DNA extraction by successive treatments with RNase and proteinase K, viral genomes were quantified by a real-time PCR assay using SYBR *Premix Ex Taq* (TaKaRa Bio). The real-time PCR was carried out for 40 cycles, with each cycle consisting of 95°C for 5 sec, 60°C for 10 sec, 72°C for 10 sec, and 75°C for 10 sec. Oligonucleotide primers for this assay were 5′-CTCTAGAGGATCCGGTACTCGAGGAAC-3′ (SD/SA sites) and 5′-AGAGGAGTCCAGAAGAGTGTCTCAGCC-3′ (human α-SG gene) for the α-SG gene in the rAAV2 genome and 5′-TGCCATGAGCAGCCCATTTTG-3′ and 5′-ATAACATCGCGGTGGCTCAGG-3′ for the slug promoter. The slug promoter was used for normalization of data across samples.

Analysis of toxicity

Blood was obtained from a murine heart. Serum alanine aminotransferase, γ-glutamyl transpeptidase, albumin, and total protein concentration were determined with a Fuji Dri-Chem slide system (Fujifilm, Tokyo, Japan).

Muscle physiological function

TA and extensor digitorum longus (EDL) muscles were exposed by removal of overlying connective tissue (Xiao *et al.*, 2000; Yoshimura *et al.*, 2004; Imamura *et al.*, 2005). Both tendons of the TA and EDL muscles were cut from their insertions and secured with 5-0 silk sutures. Muscles were mounted in a vertical tissue chamber containing physiological salt solution (150 m*M* NaCl, 4 m*M* KCl, 1.8 m*M* $CaCl_2$, 1 m*M* $MgCl_2$, 5 m*M* HEPES, 5.6 m*M* glucose [pH 7.4], and 0.02 m*M* D-tubocurarine) maintained at 37°C with continuous aeration. The chamber was connected to a force transducer (UL-10GR; Minerva, Nagano, Japan) and a length servosystem (MM-3; Narishige, Tokyo, Japan). Electrical stimulation (SEN3301; Nihon Kohden, Tokyo, Japan) was delivered through a pair of platinum wires placed on both sides of the muscle. The muscle fiber length was adjusted incrementally with a micropositioner until peak isometric twitch force responses were obtained (i.e., optimal fiber length L_o). L_o was measured with a microcaliper. Maximal tetanic force (P_o) was induced by stimulation frequencies of 125 pulses per second, delivered in trains of 500-msec duration with 2-min intervals between each train. The muscle was weighed, rapidly frozen in liquid nitrogen-cooled isopentane, and stored at –80°C for further analysis. All forces were normalized to the physiological cross-section area (CSA), which was estimated on the basis of the following formula: muscle wet weight (in mg)/[L_o (in mm) × 1.06 (in mg/mm^3)]. The estimated CSA was used to determine specific tetanic (P_o/CSA) force of the muscle. Data are presented as means ± SE. Differences between groups were assessed by Student *t* test.

Exercise tolerance tests

Mice were subjected to an exhaustion treadmill test (Mourkioti *et al.*, 2006). Each mouse was placed on the belt of a four-lane motorized treadmill (MK-680; Muromachi Kikai, Tokyo, Japan) supplied with shocker plates. The treadmill was run at an inclination of 7 degrees at 5 m/min for 5 min, after which the speed was increased by 1 m/min every minute. The test was terminated when the mouse remained on the shocker plate for more than 20 sec without attempting to reengage the treadmill, and the time to exhaustion was determined.

Results

Expression of α-SG after injection of rAAV2- or rAAV8-α-SG into TA muscles of neonatal α-SG-deficient mice

We constructed rAAV2- and rAAV8-α-SG expressing human α-SG cDNA under the control of the ubiquitous CMV promoter, and injected 1×10^{11} VG into the right TA muscle of neonatal Sgca$^{-/-}$ mice (Fig. 1A). Neonatal Sgca$^{-/-}$ mice showed no obvious dystrophic changes, whereas adult (>4 weeks old) Sgca$^{-/-}$ skeletal muscles showed active cycles of the degeneration–regeneration process. In the hind limb muscles of 5-week-old Sgca$^{-/-}$ mice, α-SG-positive

TABLE 1. EFFECT OF rAAV2- AND rAAV8-α-SARCOGLYCAN ADMINISTRATION ON THE LIVER FUNCTION OF ADULT Sgca$^{-/-}$ MICE 4 WEEKS AFTER INJECTION[a,b]

	Number of mice	*ALT (U/liter)*	*γ-GTP (U/liter)*	*ALB (g/dl)*	*TP (g/dl)*
Sgca$^{+/+}$	3	26.67 ± 8.50[c]	<10	2.43 ± 0.21	4.80 ± 0.20
Sgca$^{-/-}$	3	145.33 ± 22.22	<10	2.33 ± 0.23	4.60 ± 0.42
rAAV2-injected Sgca$^{-/-}$	3	149 ± 9[d]	<10	2.10 ± 0.44	4.00 ± 0.53
rAAV8-injected Sgca$^{-/-}$	3	124 ± 15.10[e]	<10	2.03 ± 0.25	4.60 ± 0.89

Abbreviations: ALT/GPT, alanine aminotransferase/glutamic pyruvic transaminase; γ-GTP, γ-glutamyl transpeptidase; ALB, albumin; TP, total protein.

[a]Data represent means ± SE.

[b]The *p* values indicate statistical significance. Significant differences from the ALT/GPT level of Sgca$^{-/-}$ mice are indicated.

[c]$p < 0.001$.

[d]$p = 0.797$.

[e]$p = 0.229$.